Space-charge dynamics in photorefractive polymers

Oksana Ostroverkhova[a] and Kenneth D. Singer[b]
Department of Physics, Case Western Reserve University, Cleveland, Ohio 44106-7079

(Received 6 May 2002; accepted for publication 9 May 2002)

The model of space-charge formation in photorefractive polymers due to Schildkraut and Buettner has been modified to include thermally accessible deep traps as well as shallow traps. The dynamic equations have been solved semiempirically using independent measurements of photoconductive properties to predict photorefractive dynamics. Dependencies of the dynamics on charge generation, mobility, trap density, acceptor density, ionized acceptor density, as well as their associated rates are examined. The magnitude of the fast time constant of photorefractive development is successfully predicted. The introduction of deep traps into the model has allowed us to qualitatively predict the reduction in speed due to deep trap filling and ionized acceptor growth. Experimental studies of photoconductivity and photorefraction (PR) in several polyvinyl carbazole photorefractive composites are carried out to demonstrate the applicability of the model. By choosing chromophores with different ionization potentials and by varying the chromophore concentrations, we investigate the influence of the chromophore ionization potential on the photoelectric and PR properties and reveal the nature of deep traps in the composites and their contribution to both photoconductivity and PR dynamics. Effects of plasticizer components are also discussed. [DOI: 10.1063/1.1491279]

I. INTRODUCTION

The photorefractive (PR) effect involves a change in refractive index in an electro-optical material resulting from the redistribution of charge carriers created under the influence of optical beams. This mechanism results in a process, where the phase shift between the incident intensity pattern and resulting refractive index pattern due to Poisson's equation leads to a number of useful nonlinear optical phenomena of interest for image and data processing and storage. The specific processes required for the PR effect include: photogeneration of charge carriers, transport of mobile carriers, trapping of these carriers in the regions of destructive interference and a change of the refractive index in response to space-charge field. Considerable effort has been applied in order to understand the influence of each of these processes on the PR performance in a variety of materials.

Organic and polymeric materials have been the subject of numerous recent studies. In these materials, several groups have addressed these photoelectric mechanisms, especially photogeneration and transport. Photogeneration efficiency is usually probed using the xerographic discharge technique[1–3] or is estimated from dc photoconductivity,[4] while charge carrier mobility is measured using the time-of-flight or holographic time-of-flight techniques.[5,6] Charge trapping mechanisms in PR polymers are still not clearly understood, although several techniques such as two-beam coupling,[7] absorption spectroscopy,[8] and comparison of external photocurrent efficiency to the photogeneration efficiency[3] have been used to study the nature of traps. The mechanisms of space-charge field-induced refractive index change has been investigated by ellipsometric[9–12] and electric field-induced second harmonic generation[13] experiments.

Since polymeric PR materials are potentially useful for a number of applications that require fast response times, PR dynamics is an important subject for investigation. Recently, a number of studies have been aimed at understanding the relationship between photoconductivity and PR speed[4,14,15] and to develop a theory describing grating formation.[16,17] However, a systematic theoretical study of photoconductive mechanisms in PR speed in polymers has not been carried out, as has been for steady-state PR.[3,18] Even for steady-state PR, only the limiting cases of deep traps or no traps are usually considered, although the presence of shallow traps has been confirmed both by the dispersive nature of charge transport in these disordered media[19,20] and by the sublinear intensity dependence of the PR grating erasure rate.[21]

In the theoretical part of this article, we modify Schildkraut and Buettner's[16] model to take into account both shallow and thermally accessible deep traps. We then use a semiempirical technique to solve the dynamical and constitutive equations of the model to predict the dynamic PR response from independently measured photoelectric properties. In particular, we obtain the trapping, detrapping, and recombination properties of the material from the dynamics of dc photoconductivity, and use them in combination with measurements of charge generation and mobility to reveal the PR dynamics. By performing numerical simulations, we explore the dependence of the PR speed on all of these photoconductive parameters. The introduction of thermally accessible deep traps into the model has allowed us to fully characterize the PR dynamic, and to access their consequences. Thus we are able to describe the observed growth of radical C_{60}^{-} (ionized acceptors) in various materials[8,22] as well as the PR response time fatigue due to sample illumination prior to PR

[a]Present address: Department of Chemistry, Stanford University, Stanford, CA 94305-5080.
[b]Electronic mail: kds4@po.cwru.edu

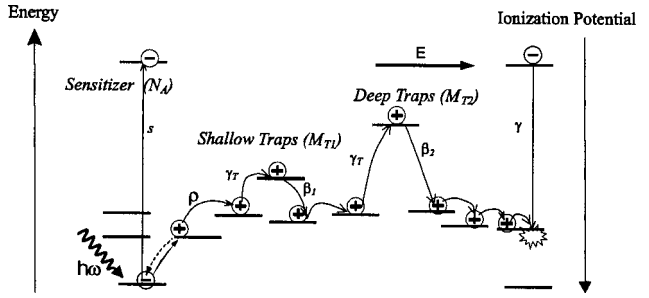

FIG. 1. Schematic representation of the modified model for photorefractive polymers. Symbols are E: electric field, ω: frequency of light, ρ: free charge density, s: photogeneration cross section, γ_T: trapping rate, γ: recombination rate, and $\beta_{1,2}$: detrapping rates.

measurements.[22] Our aim is to provide a useful experimental and numerical modeling process for predicting PR dynamics from basic material properties in order to guide the development of new materials.

In the experimental part of this article, we assess the applicability of the modified model and examine the contribution of chromophores and plasticizers to photoconductive and photorefractive performance of PR polymers. We address how the PR-relevant photoelectric properties such as mobility, charge generation efficiency, trapping, detrapping, and recombination rates are influenced by the degree of disorder, trap depths, ionization potentials of the constituents, presence of ionic impurities, etc. We analyze the photoconductive and photorefractive behavior of both plasticized[4,11,14] and unplasticized polyvinyl carbazole (PVK) composites including the sensitizer (C_{60}) and several chromophores. For composites of both classes, we determine the quantum efficiency, mobility, trapping, detrapping, and recombination rates from photoelectric measurements. Then using these rates we (i) calculate the PR speed as determined by four-wave mixing, (ii) compare corresponding rates for different chromophores and relate them to relevant ionization potentials, (iii) study the influence of plasticizer on photoconductivity and photorefractive performance of the composite, and finally, (iv) study the nature of shallow and deep traps in composites and investigate their influence on photoconductive and photorefractive properties of the materials.

II. THEORY

The first theoretical description of PR in polymers was adapted from Kukhtarev's[23] theory of inorganic crystals by Schildkraut and Buettner.[16] They included the rate equation for traps in the system of PR dynamical equations and took into account the field dependence of both photogeneration of mobile carriers and mobility. The modified model presented here differs from Schildkraut and Buettner's by introducing two kinds of traps—shallow and deep. Here, by the term ''deep,'' we mean that the rate of thermal detrapping for these traps is at least an order of magnitude lower than that of shallow traps, but still having a nonzero probability for detrapping. The processes taken into account in here are depicted in Fig. 1. A sensitizer (acceptor) with density N_A is excited and subsequently ionized by light of frequency ω with cross-section s. A free hole is injected into the transport manifold and hops between transport sites until it either becomes trapped or recombines with ionized acceptors with rate γ. Although, generally, the energy spectrum of trapping sites has a continuous distribution,[21] for tractability we consider only two kinds of traps with well-defined energy levels (ionization potential)—shallow traps M_{T1} and deep traps M_{T2}. We assume that the trapping rate does not depend on the trap depth,[24,25] so that shallow and deep traps are filled with the same trapping rate γ_T. Detrapping proceeds with a thermal excitation rate β_1 for shallow traps or β_2 for deep traps. Optical detrapping is not considered because the depth of both shallow and deep traps (<0.5 eV) is much smaller than the photon energy $\hbar\omega$ (~ 1.96 eV for HeNe 633 nm light). Then, the modified system of nonlinear equations describing the PR dynamics is given by

$$
\begin{aligned}
&\frac{\partial \rho}{\partial t} = \frac{\partial N_A^i}{\partial t} - \frac{\partial M_1}{\partial t} - \frac{\partial M_2}{\partial t} - \frac{1}{e}\frac{\partial J}{\partial x},\\
&\frac{\partial M_1}{\partial t} = \gamma_T (M_{T1} - M_1)\rho - \beta_1 M_1,\\
&\frac{\partial M_2}{\partial t} = \gamma_T (M_{T2} - M_2)\rho - \beta_2 M_2,\\
&\frac{\partial N_A^i}{\partial t} = sI(N_A - N_A^i) - \gamma N_A^i \rho,\\
&\frac{\partial E}{\partial x} = \frac{e}{\epsilon_0 \epsilon}(\rho + M_1 + M_2 - N_A^i),\\
&J = e\mu\rho E - e\mu\xi\frac{\partial \rho}{\partial x}.
\end{aligned}
\tag{1}
$$

Here ρ is the free charge (hole) density, N_A the total density of acceptors (e.g., C_{60}), N_A^i the density of ionized acceptors (e.g., C_{60}^-), M_1, M_2, M_{T1}, and M_{T2} the densities of filled shallow traps, filled deep traps, and total shallow and deep trapping sites, respectively, E the electric field, and I the incident light intensity. J is the current density, μ the charge carrier drift mobility, and ξ is the diffusion coefficient given by $\xi = k_B T/e$. The quantity s is the cross section of photogeneration, γ_T, β_1, β_2 the trapping rate and detrapping rates for shallow and deep traps, respectively, γ the recombination rate, and ϵ the dielectric constant. We consider the parameters s, μ, γ_T, and γ to be electric field dependent assuming the following dependencies:[18]

$$
\begin{aligned}
&s = s(E_{\mathrm{ref}})(E/E_{\mathrm{ref}})^p,\\
&\mu = \mu(E_{\mathrm{ref}}) e^{\beta_\mu (E^{1/2} - E_{\mathrm{ref}}^{1/2})},\\
&\gamma = \gamma(E_{\mathrm{ref}}) e^{\beta_\mu (E^{1/2} - E_{\mathrm{ref}}^{1/2})},\\
&\gamma_T = \gamma_T(E_{\mathrm{ref}}) e^{\beta_\gamma (E^{1/2} - E_{\mathrm{ref}}^{1/2})}.
\end{aligned}
\tag{2}
$$

Here E_{ref} is the relevant reference electric field for each of the parameters. During photorefractive grating formation, the reference electric field for photogeneration efficiency is the external applied field, while for mobility, trapping, and re-

combination rates the reference electric field is the projection of the applied field on the grating vector. Parameters p, β_γ, and β_μ are determined experimentally.

Since the creation of a photorefractive hologram assumes a nonuniform light intensity pattern created by the interfering beams, the incident light intensity can be expressed as a periodic function of x:

$$I = I_0 + I_1 \cos kx, \tag{3}$$

where k is the grating vector chosen to be parallel to the x direction. The general spatial dependence of Eq. (3) will also apply to the response of the polymeric material. The exact electric field and charge density distributions must be determined by numerically solving Eqs. (1)–(3). However, as shown by Schildkraut and Cui[18] for the steady state, the numerically determined values for free charge density and the amplitude and phase of the space-charge field were in a good agreement with the corresponding values obtained from the Fourier analysis of the equations analogous to our Eq. (1). Also, the Fourier decomposition approach was used by Cui *et al.* for the analysis of dynamics of the PR grating erasure.[21] So, as we proceed, we use a Fourier decomposition of all the densities, electric field, and current and separate the equations on the basis of the spatial dependence of the terms. We also consider the case of moderate applied electric fields ($E_a < 50\ \mathrm{V}/\mu\mathrm{m}$), where effects of grating bending and higher spatial harmonics can be neglected,[26] and thus limit our analysis to the zeroth and first spatial Fourier components. We experimentally investigated the dependence of the PR dynamics on the intensity modulation depth $m = I_1/I_0$. We found that in contrast with a steady-state PR performance, the PR dynamics observed under our experimental conditions of short prior-to-experiment light exposure time of ~ 10 s and total writing beam intensities below 400 $\mathrm{mW/cm^2}$ depended only on I_0 rather than the modulation depth m, as expected from the theory for the first spatial order Fourier decomposition. Therefore in our range of electric fields and incident intensities, the PR dynamics did not depend on the modulation depth, and thus, the unity modulation depth (a conventional choice of experimental geometry in PR polymer literature), is used in this article. Then, the solution of Eq. (1) can be written in the following form:

$$\zeta = \zeta_0(t) + \zeta_1(t)(C_{\zeta 1} \cos kx + C_{\zeta 2} \sin kx), \tag{4}$$

where $\zeta = \rho, M_1, M_2, N_A^i, J$. Since the mobility and all of the relevant charge generation, trapping, and recombination rates are field-dependent, we assume a form similar to Eq. (4) for each of these parameters as well as for the electric field E with time-independent ζ_0.[18] We substitute Eq. (4) in Eq. (1) and separate the spatially independent zeroth order and spatially varying first order systems of equations. We start from the zeroth order equations that describe photoconductivity in PR polymers under homogeneous illumination of intensity I_0. As we proceed, we will use our photoconductivity experiments and theory (zeroth order) to predict the PR dynamics (first order) assuming that the influence of Gaussian rather than uniform incident beams is the same for both zeroth and first order processes.

A. Zeroth order: Photoconductivity in photorefractive polymers

In this section we explore how the information about rates relevant for PR grating formation can be extracted from the photocurrent dynamics. The zeroth order system of equations derived from Eq. (1) is written as follows:

$$\begin{aligned}
\frac{dM_{10}(t)}{dt} &= \gamma_T(E_0)[M_{T1} - M_{10}(t)]\rho_0(t) - \beta_1 M_{10}(t), \\
\frac{dM_{20}(t)}{dt} &= \gamma_T(E_0)[M_{T2} - M_{20}(t)]\rho_0(t) - \beta_2 M_{20}(t), \\
\frac{dN_{A0}^i(t)}{dt} &= s(E_0) I_0 [N_A - N_{A0}^i(t)] - \gamma(E_0) N_{A0}^i(t) \rho_0(t), \\
\rho_0(t) &+ M_{10}(t) + M_{20}(t) - N_{A0}^i(t) = 0.
\end{aligned} \tag{5}$$

One more equation that is not included in Eq. (5) but provides a link to dc photoconductivity experiments is the constitutive equation for the photocurrent $J_0(t)$ given by $J_0(t) = e\mu(E_0)\rho_0(t)E_0$. Equation (5) describes the dynamics of free charge generation followed by transport, trapping, detrapping, and recombination in the photorefractive polymers under external electric field E_0. We consider the electric field E_0 to be constant and given by $E_0 = V/d$, where V is the applied voltage and d is the thickness of the polymeric film. Then, the time evolution of the photocurrent $J_0(t)$ probes the dynamics of free charge density $\rho_0(t)$ that is connected through Eq. (5) to the generation, trapping, detrapping, and recombination processes in the PR polymers. The rates describing these processes $(s, \gamma_T, \beta_{1,2}, \gamma)$ are intrinsic characteristics of the polymer composites, and our goal is to determine their influence on both photoconductivity and photorefractive speed. It should also be mentioned that since all the rates are electric-field dependent, the photoconductivity experiments have to be conducted in the range of external electric field E_0 that covers both applied electric field in PR experiment E_a and its projection on the grating vector $\tilde{E}_a$ in order to proceed with calculating the space-charge field dynamics (first order) on the basis of parameters determined from the photoconductivity (zeroth order).

To study the temporal behavior of the free charge ρ, trapped charge M_1, M_2, and ionized acceptor N_A^i densities, it is convenient to transform Eq. (5) to a dimensionless form. The time scale is normalized by the average drift time of the free carrier before it is trapped by a shallow trap: $\tau = t/\tau_0$, where $\tau_0 = 1/[\gamma_T(E_0)M_{T1}]$. The reason for this choice of time scale will be explained later in the Sec. II A 1. We express all the densities in terms of total acceptor density N_A: $\varrho = \rho/N_A$, $m_{T1,2} = M_{T1,2}/N_A$, $m_{1,2} = M_{1,2}/N_A$, and $n_A^i = N_A^i/N_A$. We also introduce the relative photogeneration, recombination, and detrapping parameters $\tilde{s}I_0 = sI_0\tau_0$, $\tilde{\gamma} = \gamma\tau_0 N_A$, and $\tilde{\beta}_{1,2} = \tau_0\beta_{1,2}$, respectively. The dimensionless analog of Eq. (5) is then written as follows:

$$\begin{aligned}
\frac{dm_{10}}{d\tau} &= \left(1-\frac{m_{10}}{m_{T1}}\right)\varrho_0 - \tilde{\beta}_1 m_{10},\\
\frac{dm_{20}}{d\tau} &= \frac{m_{T2}}{m_{T1}}\left(1-\frac{m_{20}}{m_{T2}}\right)\varrho_0 - \tilde{\beta}_2 m_{20},\\
\frac{dn^i_{A0}}{d\tau} &= \tilde{s}I_0(1-n^i_{A0}) - \tilde{\gamma} n^i_{A0}\varrho_0,\\
\varrho_0(\tau) &+ m_{10}(\tau) + m_{20}(\tau) - n^i_{A0}(\tau) = 0.
\end{aligned} \tag{6}$$

This is a nonlinear system that cannot be solved analytically. However, we can consider different cases depending on the total trap densities with respect to the acceptor density in the material, leading to simplifications of these equations.

Case 1. Both the total shallow and deep trap densities are smaller or on the order of the acceptor density: $m_{T1,2} \lesssim 1$.

Case 2. The total deep (shallow) trap density is smaller or on the order of the acceptor density, but the total shallow (deep) trap density is much larger than the acceptor density: $m_{T2} \lesssim 1$, $m_{T1} \gg 1$ or vice versa. In this case, the ratio $m_{10}/m_{T1} \ll 1$ (or $m_{20}/m_{T2} \ll 1$) is always valid, and the first (second) equation in Eq. (6) is simplified.

Case 3. Both deep and shallow total trap densities are much larger than the acceptor density: $m_{T1,2} \gg 1$. In this case both ratios $m_{10}/m_{T1} \ll 1$ and $m_{20}/m_{T2} \ll 1$ are always valid, so that both the first and second equations in Eq. (6) become linear.

Our simulations show that in the trap-limited regime (*Case 1*) photocurrent dynamics is similar to the short-time scale regime of *Cases 2,3* (Sec. II A 1). *Case 1* does not describe long-time scale changes in both photocurrent and space-charge field, and therefore, seems not to be applicable for most of our materials. Therefore we consider only *Case 2* and *Case 3*, which can be applicable depending on the chromophore ionization potential and concentration.[27,28] We start our analysis from *Case 3* and then extend it to *Case 2*.

1. Trap-unlimited regime

In this section we consider the case when the total density of both shallow and deep traps is much higher than the acceptor density $m_{T1,2} \gg 1$ (*Case 3*). Then, Eq. (6) is simplified to

$$\begin{aligned}
\frac{dm_{10}}{d\tau} &= \varrho_0 - \tilde{\beta}_1 m_{10},\\
\frac{dm_{20}}{d\tau} &= \frac{m_{T2}}{m_{T1}}\varrho_0 - \tilde{\beta}_2 m_{20},\\
\frac{dn^i_{A0}}{d\tau} &= \tilde{s}I_0(1-n^i_{A0}) - \tilde{\gamma} n^i_{A0}\varrho_0,\\
\varrho_0(\tau) &+ m_{10}(\tau) + m_{20}(\tau) - n^i_{A0}(\tau) = 0.
\end{aligned} \tag{7}$$

We also assume that the density of total shallow traps is much larger than the density of total deep traps $m_{T1} \gg m_{T2}$ which seems to be relevant for all the composites we studied (Sec. III A). Then, we can separately consider different time scales at which either shallow (''short time scale'') or deep (''long time scale'') trap dynamics prevails in order to provide insight into the experimentally observed trapping, detrapping, and recombination rates as deduced from dc photoconductivity.

a. Short time scale. On the short time scale, the dynamics of the system is entirely determined by shallow traps. To probe the behavior of our system, we first consider the initial rise in photocurrent as the nonlinear term $\tilde{\gamma}\varrho_0 n^i_{A0}$ in the third equation of Eq. (7) is much smaller than the linear term $\tilde{s}I_0 n^i_{A0}$ in that same equation. This transforms the nonlinear system of Eq. (7) into a linear one that can be solved analytically. Then, we seek a solution of the form $\varsigma = \varsigma_0 e^{-\tilde{\lambda}\tau}$, where $\varsigma = m_{10}, m_{20}, n^i_{A0}$, and then solve for the three characteristic rates $\tilde{\lambda}$ that determine the dynamics of dc photoconductivity at this time scale: $\tilde{\lambda}_1 = 1 + m_{T2}/m_{T1} \approx 1$; $\tilde{\lambda}_2 = \tilde{s}I_0$; and $\tilde{\lambda}_3 \approx \tilde{\beta}_2 + (m_{T2}/m_{T1})\tilde{\beta}_1$. In these equations we assume that the detrapping parameters $\tilde{\beta}_1$ and $\tilde{\beta}_2$ are much smaller than 1 and (m_{T2}/m_{T1}), respectively. This assumption holds when the free charge density is much smaller than the density of filled traps as observed in a variety of materials.[3,29] We have also confirmed this in our photoconductivity experiment for materials described here. For this reason and also in keeping with our experimental observations that the charge generation rate at reasonable experimental intensities $I_0 < 1$ W/cm^2 is much smaller than the trapping parameter $1/\tau_0$, i.e., $\tilde{s}I_0 \ll 1$ (Sec. IV A 1), we can assume that $\tilde{\lambda}_2 \ll \tilde{\lambda}_1$ and $\tilde{\lambda}_3 \ll \tilde{\lambda}_1$.

Thus the fastest photoconductivity dynamics is given by unity $\tilde{\lambda}_1 \approx 1$ in the dimensionless form. This fact explains our choice of the time scale being normalized with respect to $\tau_0 = 1/(\gamma_T M_{T1})$. Thus in dc photoconductivity experiments the fastest photocurrent dynamics $[J_0(t) \sim \rho_0(t)]$ is determined by the value for the shallow trapping product $\gamma_T M_{T1}$.

In the next longer time regime (though still in the shallow trapping fast limit) we need to consider that, as we will see later, the free charge density has reached a maximum and starts to decrease. Then, we can replace the free charge density function $\varrho_0(\tau)$ in the nonlinear term of the third equation in Eq. (7) with a quasi-steady value $\overline{\varrho_0}$. We again obtain three time constants out of which $\tilde{\lambda}_2$ is of relevance and given by $\tilde{\lambda}_2 = \tilde{s}I_0 + \tilde{\gamma}\overline{\varrho_0}$. In this intermediate time regime, $\tilde{\lambda}_2$ contains information regarding the recombination parameter $\tilde{\gamma}$.

Summarizing the dynamics of the photoconductivity on a short time scale (for PVK-based materials we studied, this corresponds to $\tau \lesssim 50$), we obtain the following expressions for dc photoconductivity rates: $\tilde{\lambda}_1 \approx 1$; $\tilde{\lambda}_2 = \tilde{s}I_0 + \tilde{\gamma}\overline{\varrho_0}$. In keeping with our experiments, in the low intensity regime (below 1 W/cm^2), we can simplify these to $\tilde{\lambda}_1 \approx 1$; $\tilde{\lambda}_2 \approx \tilde{\gamma}\overline{\varrho_0}$.

Thus in dc photoconductivity experiments, the short time scale dynamics can be fitted with a biexponential function, where the faster rate λ_1 yields the shallow trapping product $\gamma_T M_{T1}$, and the slower rate λ_2 is directly related to the recombination rate γ.

To test our approximations, we performed numerical simulations fixing $\tilde{s}I_0 = 10^{-2}\tau_0$, $m_{T2}/m_{T1} = 0.1$, $\tilde{\beta}_1$

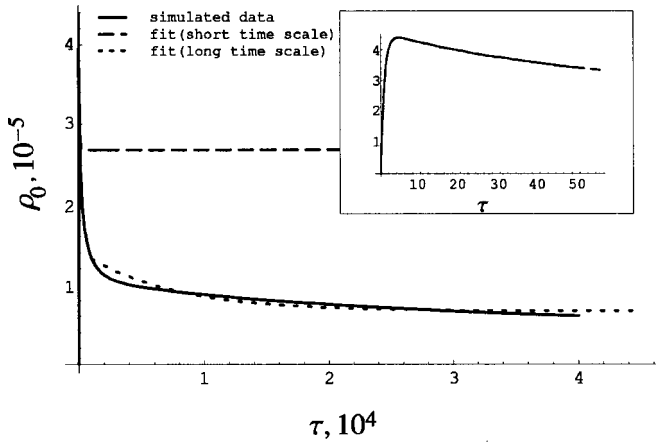

FIG. 2. Simulated dynamics of dc photocurrent for the case $m_{T1} \gg m_{T2} \gg 1$ using Eq. (7) and parameters $\tilde{s}I_0 = 5\times10^{-5}$, $m_{T2}/m_{T1} = 0.1$, $\tilde{\beta}_1 = 5\times10^{-4}$, $\tilde{\beta}_2 = 5\times10^{-6}$, and $\tilde{\gamma} = 2.5\times10^2$. The inset shows the short time scale part of the photocurrent transient (data and fit).

$=0.1\tau_0$, $\tilde{\beta}_2 = 0.001\tau_0$, and varying the average carrier lifetime τ_0 and the recombination parameter $\tilde{\gamma}$. This choice of parameters used for the simulation was suggested by the corresponding typical values observed experimentally in unplasticized composites (Sec. IV A 1). First, at $\tilde{\gamma} = 5\times10^4\tau_0$ we substituted different values of the parameter τ_0 into Eq. (7), and numerically solved this system to find the dependence of $\varrho_0(\tau)$ for $\tau \leqslant 50$. At this time scale, the free charge density grows as the charge is injected into the transport manifold, reaches the maximum $\varrho_{0,\max}$, and then decreases, due to recombination and trapping. We then fit the calculated curve of the free charge density $\varrho_0(\tau)$ with a biexponential function

$$\varrho_{\text{fit}} = A(1 - Be^{-\tilde{\lambda}_{10}\tau} + (B-1)e^{-\tilde{\lambda}_{20}\tau}) \tag{8}$$

to determine $\tilde{\lambda}_{10}$ (the faster constant) and compare it to $\tilde{\lambda}_1 = 1$. At $B > 1$ Eq. (8) describes the photocurrent rise with the rate $\tilde{\lambda}_{10}$ and then the photocurrent decay with the rate $\tilde{\lambda}_{20}$. We found that the faster constant in the biexponential fit yields values equal to unity within 10%, as anticipated. To extract the slower rate, we used a fixed $\tau_0 = 5$ ms (typical value for an unplasticized sample observed in dc photoconductivity experiment at $E_0 \sim 30\ \text{V}/\mu\text{m}$ and $I_0 \sim 50\ \text{mW/cm}^2$) for different recombination parameters $\tilde{\gamma}$, found $\varrho_0(\tau)$, and fit it using Eq. (8) to determine $\tilde{\lambda}_{20}$. We found that $\tilde{\lambda}_{20}$ agrees with $\lambda_2 = \tilde{\gamma}\varrho_0(\varrho_0 = \varrho_{0,\max})$ within a factor of 3. As we show in Ref. 28 and mention later in Sec. II B 1, an error of this magnitude in the recombination rate actually has a negligible effect on the PR speed. This agreement is remarkable since we dealt so crudely with the nonlinear term containing the charge density.

As an example, consider the dynamics of the dc photocurrent simulated using the parameters $\tilde{s}I_0 = 5\times10^{-5}$, $m_{T2}/m_{T1} = 0.1$, $\tilde{\beta}_1 = 5\times10^{-4}$, $\tilde{\beta}_2 = 5\times10^{-6}$, and $\tilde{\gamma} = 2.5\times10^2$ (solid line in Fig. 2). The dashed line in the figure is a biexponential fit of the short time behavior using Eq. (8). The faster inverse time constant of this fit $\tilde{\lambda}_{10} = 1.1$ reflects the expected value of $1 + m_{T2}/m_{T1} = 1.1$. The slower speed $\tilde{\lambda}_{20} = 1.9\times10^{-2}$ divided by the dimensionless free charge density in its maximum $\varrho_{0,\max} \approx 4.4\times10^{-5}$ yields, according to $\tilde{\lambda}_{20} = \tilde{\gamma}\varrho_{0,\max}$, the recombination parameter $\tilde{\gamma} \approx 4.3\times10^2$, which is within the expected range of values given the input value $\tilde{\gamma} = 2.5\times10^2$. The biexponential of Eq. (8) fits the $\varrho_0(\tau)$ dependence perfectly at $\tau < 50$ (inset of Fig. 2), but as the processes which are not taken into account at short time scale take over at $\tau \gg 50$, the short time scale fit does not follow the photocurrent dynamics correctly (dashed line in Fig. 2), and thus long time scale analysis should be applied.

We now use a procedure to produce a better time evolution for ϱ_0 that will also yield the detrapping parameter for shallow traps. Although it is not obvious how to analytically extract the detrapping parameter for shallow traps $\tilde{\beta}_1$, $\varrho_0(\tau)$ at short time scales is rather sensitive to changes in $\tilde{\beta}_1$.[28] To find the detrapping parameter $\tilde{\beta}_1$ and to fine-tune the recombination parameter $\tilde{\gamma}$, we used the $\tilde{\gamma}$ estimated above as the initial value in Eq. (7) and varied both $\tilde{\beta}_1$ and $\tilde{\gamma}$. At every step we calculated the dimensionless free charge density $\varrho_0(\tau)$ and fit to Eq. (8). Then we transformed the dimensionless fit parameter $\tilde{\lambda}_{20}$ to the dimensional form $\lambda_{20} = \tilde{\lambda}_{20}/\tau_0$ and compared them to the analogous parameters of a biexponential fit of dc photoconductivity data. The comparison was executed by searching for a minimum of the function

$$f = \left(\frac{\lambda_{20,\text{exp}} - \lambda_{20}}{\lambda_{20,\text{exp}}}\right)^2 + \left(\frac{B_{\text{exp}} - B}{B_{\text{exp}}}\right)^2, \tag{9}$$

where $\lambda_{20,\text{exp}}$, B_{exp} are the experimental parameters analogous to corresponding parameters λ_{20}, B introduced in Eq. (8).

Summarizing the short time scale dc photoconductivity dynamics for the case $m_{T1} \gg m_{T2} \gg 1$, we are able to determine the shallow trapping parameter $\gamma_T M_{T1}$, recombination rate γ, and shallow detrapping rate β_1.

b. Long time scale. On the long time scale ($\tau > 10^3$), shallow traps have reached quasiequilibrium, and deep traps determine the dynamics of the dc photoconductivity. The dimensionless parameters to be determined here are the ratio of total deep traps with respect to shallow traps m_{T2}/m_{T1} and the thermal detrapping parameter of deep traps $\tilde{\beta}_2$. We performed a numerical simulation fixing the parameters $\tilde{s}I_0 = 5\times10^{-5}$, $\tilde{\beta}_1 = 5\times10^{-4}$, $\tilde{\gamma} = 2.5\times10^2$, and varying m_{T2}/m_{T1} (while maintaining the ratio $m_{T2}/m_{T1} \ll 1$) and $\tilde{\beta}_2$. Similar to the short time scale approach, we fit the free charge density $\varrho_0(\tau)$ with a biexponential similar to Eq. (8) (dotted line in Fig. 2). The faster speed $\tilde{\lambda}_{10}$ was kept fixed equal to unity. Then, our fit yielded two coefficients—the slower speed $\tilde{\lambda}_{20,\text{long}}$ and the exponential prefactor B_{long}. Although at this time scale, it is not straightforward to relate the constants of the fit to the parameters of the material directly, our simulations show that the deep to shallow trap density ratio m_{T2}/m_{T1} and deep detrapping parameter $\tilde{\beta}_2$ can be found from the fit constants in a manner similar to the short time scale analysis. When dealing with the experimental data, we constructed the function

$$f_1=\left(\frac{\lambda_{20,\mathrm{exp,long}}-\lambda_{20,\mathrm{long}}}{\lambda_{20,\mathrm{exp,long}}}\right)^2+\left(\frac{B_{\mathrm{exp,long}}-B_{\mathrm{long}}}{B_{\mathrm{exp,long}}}\right)^2,$$

where $\lambda_{20,\mathrm{exp,long}}$ and $B_{\mathrm{exp,long}}$ are the experimental constants analogous to $\lambda_{20,\mathrm{long}}=\lambda_{20,\mathrm{long}}/\tau_0$ and B_{long}. Similar to the short time scale approach, we sought values for m_{T2}/m_{T1} and $\tilde{\beta}_2$ that would minimize the function f_1.

Summarizing the long time scale dc photoconductivity dynamics for the case $m_{T1}\gg m_{T2}\gg 1$, we are able to experimentally determine the product $\gamma_T M_{T2}$ and the detrapping rate β_2.

2. Trap-limited regime

In this section, we consider the dc photoconductivity dynamics when the total density of traps is on the order or less than the acceptor density. We will limit our discussion to the case when the regime is ''trap-limited'' only with respect to deep traps (*Case 2*) that appears to be relevant for the materials we studied.[28] So, further in this section we assume that $m_{T1}\gg 1$ and $m_{T2}\leqslant 1$. In this case, the condition $m_{T1}\gg m_{T2}$ is satisfied automatically and thus the time scale division onto ''short'' and ''long'' is still appropriate. Also, since for shallow traps the condition $m_{T1}\gg 1$ is the same as in the previous Sec. II A 1, all the short time scale considerations are valid. However, long time scale behavior is no longer the same as in the trap-unlimited regime, mainly because in this case the condition $m_{20}/m_{T2}\ll 1$ is no longer valid, so Eq. (6) with the first equation replaced with the first equation of Eq. (7) has to be solved. Modified in this way, the system of Eq. (6) contains one more parameter than Eq. (7), so that it is not enough to determine the ratio m_{T2}/m_{T1} because of m_{T2} in the term m_{20}/m_{T2}. Our simulations show that if $m_{T2}\sim 1$ then the use of simplified Eq. (7) instead of Eq. (6) is still possible which allows us to determine the ratio m_{T2}/m_{T1} within 10% error. However, if $m_{T2}<1$, then the modified Eq. (6) must be solved since the error becomes $>100\%$. This complicates the analysis of the long time scale behavior. Also, when the density of total deep traps becomes of the order of 1% or less of the acceptor density ($m_{T2}\leqslant 0.01$), it appears to be impossible to detect deep traps in the material using dc photoconductivity. We simulated the long time scale evolution of the dimensionless free charge density $\varrho_0(\tau)$ with the fixed parameters $\tilde{s}I_0=5\times10^{-5}$, $\tilde{\beta}_1=5\times10^{-4}$, $\tilde{\beta}_2=5\times10^{-6}$, $\tilde{\gamma}=2.5\times10^2$, $m_{T1}=10$, and varying m_{T2} from 0.01 to 1. Figure 3(a) shows the deep-trap limited behavior of the photoconductivity for various total deep trap densities. As seen from Fig. 3(a), when $m_{T2}=0.01$, the decay of $\varrho_0(\tau)$ is less than 3% over the time scale corresponding to the experimental run of duration $\geqslant 10^3$ s for the PVK-based composites we studied (Sec. III), so that it would be hard to obtain a reliable fit to such data and thus the trap densities below 0.01 cannot be detected by this method. As mentioned before, in the case when $m_{T2}=0$ (no deep traps), the photoconductivity degradation during continuous illumination is not observed.

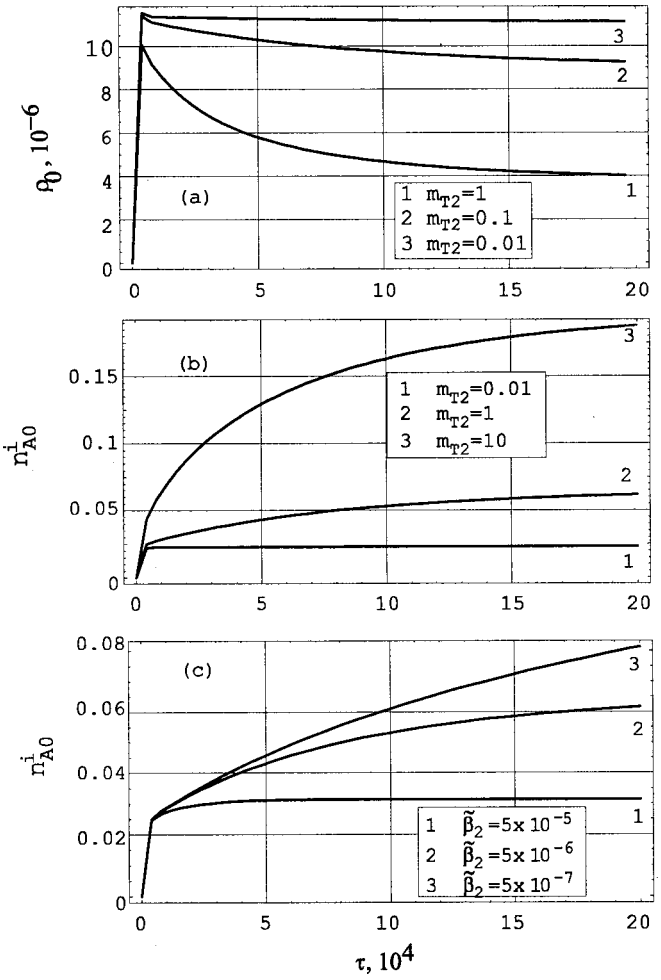

FIG. 3. Long time scale dynamics of (a) free charge density (dc photocurrent) (b) ionized acceptor number density at $\tilde{B}_2=5\times10^{-6}$ at various deep trap number densities; and (c) ionized acceptor number density at $m_{T2}=1$ at various deep trap detrapping rates, as calculated from Eq. (6) using parameters $\tilde{s}I_0=5\times10^{-5}$, $\tilde{\beta}_1=5\times10^{-4}$, $\tilde{\gamma}=2.5\times10^2$, and $m_{T1}=10$.

3. Time evolution of ionized acceptor density n^i_{A0}

According to the last equation in Eq. (5), the free charge, filled traps, and ionized acceptor densities are constrained by the charge neutrality equation, thus the photoconductivity decay, trap filling, and the growth of the density of ionized acceptors are directly connected to each other. Figure 3(b) shows the simulated time growth of the ionized acceptor density $n^i_{A0}(\tau)$ using the fixed parameters listed in the previous Sec. II A 2 and varying the total deep trap density m_{T2} from 0.01 (deep trap-limited regime) to 10 (deep trap-unlimited regime). As seen in Fig. 3(b), the more deep traps are available in the material, the more pronounced is the ionized acceptor density growth. Also, the trap depth is the factor that affects the time evolution of n^i_{A0}. Figure 3(c) shows how the depth of the traps (thermal detrapping rate) affects the formation of ionized acceptors. For this simulation we used the same parameters as for the simulation shown in Fig. 3(b), but with fixed $m_{T2}=1$ and varied $\tilde{\beta}_2$ from 5×10^{-7} to 5×10^{-5}.

Our simulations show that the steady-state number density of ionized acceptors (N^i_{A0}) in the material depends on all

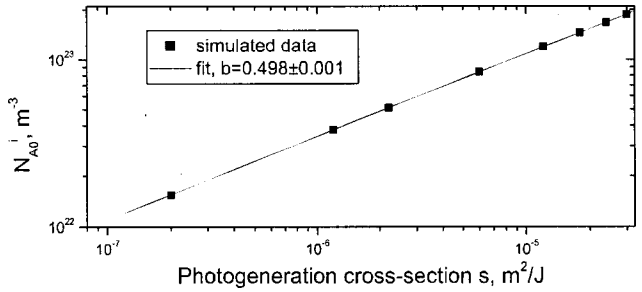

FIG. 4. Ionized acceptor number density as a function of photogeneration cross section as simulated using Eq. (6) with parameters $\tilde{\beta}_1=5\times10^{-4}$, $\tilde{\beta}_2=5\times10^{-6}$, $\tilde{\gamma}=2.5\times10^2$, $m_{T1}=10$, and $m_{T2}=1$ transformed into dimensional form using $\tau_0=5$ ms and $N_A=5\times10^{24}$ m^{-3}, and fitted with a power law function $N_{A0}^i\sim s^b$.

the rates participating in the photoconductivity–photogeneration cross-section s, trapping rate γ_T, recombination rate γ, and detrapping rates $\beta_{1,2}$. In particular, Fig. 4 shows the simulated ionized acceptor density achieved in a typical unplasticized material as a function of photogeneration cross section (simulated dependence is fitted with power law $N_{A0}^i\sim s^b$, where b was determined to be ≈0.5). This dependence explains differences in the steady-state PR performance, which depends on the density of *filled* traps related to ionized acceptor density by the electric neutrality equation [the last equation of Eq. (5)], observed in the same material sensitized with different sensitizers.[30]

In summary, the density and depth of available traps as well as other photoconductivity parameters are directly responsible for the variations in the growth of ionized acceptors n_{A0}^i (e.g., C_{60}^-) experimentally observed by several groups.[8,22]

We have determined many of the parameters of Fig. 1, and, in the next section, will show how these may be used to predict the PR dynamics. Here we provide a numerical simulation of the dynamics of the free charge and ionized acceptors for materials with deep traps, and in Sec. III we consider experimental data for different PVK-based composites and discuss the nature of traps in these materials.

B. First order: Photorefraction

In this section, we consider the formation of the first spatial Fourier component of the free charge, filled traps, and ionized acceptors densities as well as space charge field and hence PR dynamics. Here it appears more convenient to use dimensional equations rather than dimensionless for easier comparison of the simulated PR dynamics with the experiment. After substitution of Eq. (4) into Eq. (1), and separately collecting terms with $\sin kx$ and $\cos kx$, we obtain a system of ten equations—eight differential equations (with respect to time) and two equations relating the space-charge field to free charge, filled traps, and ionized acceptor densities. We consider that the photogeneration cross section, mobility, recombination, and trapping rates are electric field dependent and assume the dependencies given in Eq. (2). As mentioned before, due to these field dependencies all the parameters acquire a spatially varying part upon formation of the space-charge field. Using Eq. (2) and the approach suggested by Schildkraut and Cui,[18] we can express all the rates in terms of space-charge field as follows:

$$\begin{aligned}
&s=s(E_a)[1+p(E_1/E_a)],\\
&\mu=\mu(\tilde{E}_a)[1+(1/2)\beta_\mu\tilde{E}_a^{-1/2}E_1],\\
&\gamma=\gamma(\tilde{E}_a)[1+(1/2)\beta_\mu\tilde{E}_a^{-1/2}E_1],\\
&\gamma_T=\gamma_T(\tilde{E}_a)[1+(1/2)\beta_\gamma\tilde{E}_a^{-1/2}E_1],
\end{aligned}\tag{10}$$

where E_a is the applied electric field, $\tilde{E}_a$ is the projection of the applied field on the grating vector, and E_1 is the space-charge field given in accordance with Eq. (4) by the relation $E_1=E_{11}(t)\cos kx+E_{12}(t)\sin kx$. Then, the first order system of equations describing PR dynamics is

$$\begin{aligned}
\frac{dE_{11,12}}{dt}&=-\mu\frac{e}{\epsilon_0\epsilon}\left[\left(1+\frac{\beta_\mu\tilde{E}_a^{1/2}}{2}\right)\rho_0(t)E_{11,12}(t)\right.\\
&\qquad\left.-\tilde{E}_a\rho_{11,12}(t)\mp k\xi\rho_{11,12}(t)\right],\\
\frac{dM_{11,12}}{dt}&=\gamma_T M_{T1}\left(\rho_{11,12}(t)-\frac{\beta_\gamma\tilde{E}_a^{-1/2}}{2}E_{11,12}(t)\rho_0(t)\right)\\
&\qquad-\beta_1 M_{11,12}(t),\\
\frac{dM_{21,22}}{dt}&=\gamma_T M_{T2}\left(\rho_{11,12}(t)-\frac{\beta_\gamma\tilde{E}_a^{-1/2}}{2}E_{11,12}(t)\rho_0(t)\right)\\
&\qquad-\beta_2 M_{21,22}(t),\\
\frac{dN_{A11}^i}{dt}&=sN_AI_1-[sI_0+\gamma\rho_0(t)]N_{A11}^i(t)-\gamma N_{A0}^i(t)\rho_{11}(t)\\
&\qquad-\left(sN_AI_0\frac{p}{E_a}-\gamma\frac{\beta_\mu\tilde{E}_a^{-1/2}}{2}\rho_0(t)N_{A0}^i(t)\right)E_{11}(t),
\end{aligned}\tag{11}$$

$$\begin{aligned}
\frac{dN_{A12}^i}{dt}&=-[sI_0+\gamma\rho_0(t)]N_{A12}^i(t)-\gamma N_{A0}^i(t)\rho_{12}(t)\\
&\qquad-\left(sN_AI_0\frac{p}{E_a}-\gamma\frac{\beta_\mu\tilde{E}_a^{-1/2}}{2}\rho_0(t)N_{A0}^i(t)\right)E_{12}(t),\\
E_{11}(t)&=\frac{e}{\epsilon_0\epsilon k}[\rho_{12}(t)+M_{12}(t)+M_{22}(t)-N_{A12}^i(t)],\\
E_{12}(t)&=-\frac{e}{\epsilon_0\epsilon k}[\rho_{11}(t)+M_{11}(t)+M_{21}(t)-N_{A11}^i(t)].
\end{aligned}$$

Here E_{11}, M_{11}, M_{21}, and N_{A11}^i are the time-dependent amplitudes of space-charge field, filled shallow traps, filled deep traps, and ionized acceptors, respectively. These have a spatial dependence $\cos kx$ (in-phase with the incident light illumination). The quantities E_{12}, M_{12}, M_{22}, and N_{A12}^i are the corresponding amplitudes of functions with a spatial dependence $\sin kx$ (90° out-of-phase with the intensity of incident light).

It is conventional[16,21,29] to assume that the PR dynamics is much slower than the photoconductive dynamics, which is

analogous to setting the zeroth order $[\rho_0(t), N^i_{A0}(t)]$ functions to be constant in time in Eq. (11). In this case, Eq. (11) can be solved analytically as linear equations with constant coefficients. This approach can be applied on the short time scale. However, longer times require accounting for deep traps, which result in slowly changing components of both $\rho_0(t)$ and $N^i_{A0}(t)$, requiring Eq. (11) to be solved numerically. In the next section we will concentrate on obtaining the four wave mixing (FWM) dynamics from the theory and photoconductivity parameters.

1. Photorefractive rise

In this section we examine the factors that affect the PR rise time. First of all, it is important to perform a simulation using conditions as close as possible to a real experiment. In our case, a real experiment (FWM) is performed as follows: we turn on the electric field with one writing beam on, then in 10 s we turn on the other writing beam of the same intensity and monitor the space-charge field formation with a probe beam. In Eq. (11) that describes the PR dynamics, we need to define the behavior of zeroth order functions $\rho_0(t)$ and $N^i_{A0}(t)$, so first we simulate the time evolution of these functions under the experimental conditions described in Sec. III. The dependence of these zeroth order functions on the experimental conditions is responsible for the history dependence of the PR performance, as we will explore later in this section. So, as we determined $\rho_0(t)$ and $N^i_{A0}(t)$ for the time span of our PR experiment, we use them in Eq. (11) to simulate the evolution of the space charge field. We then calculate the diffraction efficiency,

$$\eta(t) \sim E^2_{11}(t) + E^2_{12}(t) \tag{12}$$

and fit it to a single exponential,

$$\eta = \eta_0 (1 - e^{-\nu t})^2 \tag{13}$$

where the parameter ν is PR speed. Usually in the literature, the experimentally measured diffraction efficiency is fit with a biexponential function. In this case, the initial rise is attributed to photoconductivity, and the slower one to chromophore reorientation. Thus a single exponential fit [Eq. (13)] to describe the initial space-charge field formation is adequate. This case corresponds to PR dynamics observed in our unplasticized composites. When both faster and slower experimental time constants are due to photoconductivity, which is the case for our plasticized composites, the simulated data should be fit with a biexponential function. Here, for simplicity, we consider the former case and use single exponential fits [Eq. (13)] to describe the diffraction efficiency rise due to space-charge field formation.

To explore the factors that affect the speed of space-charge field formation, we modeled the PR experiment by varying the photogeneration rate s, thermal detrapping rate β_1, recombination rate γ, total density of shallow trapping sites M_{T1}, and mobility μ. For each set of parameters we calculated PR speed ν from Eqs. (11)–(13). Although some of these parameters depend on each other and, strictly speaking, cannot be varied independently, this simulation still can provide some insight into factors determining the PR speed. Our simulation shows that the PR speed is nearly insensitive

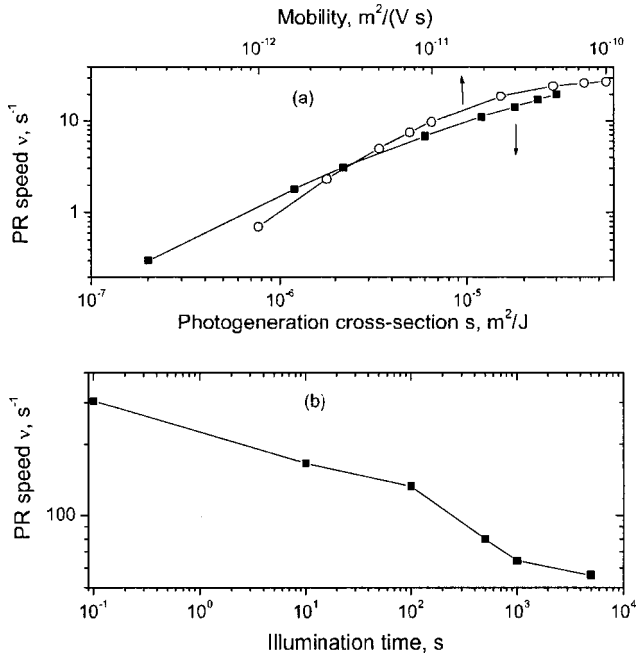

FIG. 5. Dependence of PR speed on (a) photogeneration cross section and charge carrier mobility and (b) the time of the homogeneous illumination prior to PR experiment, as calculated from Eqs. (11)–(13).

to the shallow traps release rate: the change in parameter β_1 over four orders of magnitude barely changed the PR speed by a factor of 2.[28] Larger effects were observed when changing other parameters: a decrease in the total density of shallow trapping sites of a factor of 500 led to a sixfold increase in PR speed, and a four order of magnitude decrease in the recombination rate yielded a 30-fold increase in PR speed.[28] It should be noted that a decrease in total trap density may decrease the diffraction efficiency. Thus in this case there is a trade-off between PR speed and steady-state diffraction efficiency. As shown in Fig. 5(a), the changes in mobility and photogeneration cross section had the largest impact on a PR speed. However, it should be mentioned that an independent variation of the photogeneration cross section is more justified than an independent variation of mobility, because the recombination rate is mobility-dependent and affects the PR speed the opposite way to the mobility itself. Thus, in a real system, the mobility dependence will be smaller than that shown in Fig. 5(a).

We now explore the history dependence of the PR speed. As an example, we consider a composite with deep traps that led to decay of the dc photoconductivity and the slow growth of the ionized acceptor density. The parameters used in this simulation were experimentally observed typical values for the unplasticized composite PVK/AODCST/C_{60} (Sec. IV) at an electric field of 40 V/μm and total light intensity of 1 W/cm^2.

We simulated a FWM experiment using a fresh sample and both beams being turned on simultaneously, then the same experiment after illuminating the sample with one beam for 10 s and then turning on another one and so on up to homogeneous illumination with one beam for 5000 s prior to the PR experiment. The results of the simulation are presented in Fig. 5(b) and show that there is a substantial history

dependence of the PR speed, in particular the response time degradation in materials with deep traps, as reported in previous measurements.[31,32] The material will relax back to its initial (''fresh'') state in the dark when the traps empty, and the released charge recombines with ionized acceptors. The relaxation time is mostly determined by the trap depth.

III. EXPERIMENT

A. Materials

For our experiments we chose PVK as a photoconductive polymer, C_{60} as a sensitizer, BBP as a plasticizer, and the chromophores AODCST, PDCST, and 5CB.[33] One class of composites under investigation included the molar concentrations of the following: PVK(99%)/C_{60}(1%) (composite 1, $T_g \sim 230\,^{\circ}$C) and PVK(89%)/C_{60}(1%)/NLO(10%) where NLO is a nonlinear chromophore which in our case was represented by AODCST (composite 2, $T_g \sim 133\,^{\circ}$C), PDCST (composite 3, $T_g \sim 137\,^{\circ}$C), or 5CB (composite 4, $T_g \sim 130\,^{\circ}$C). Another class had the plasticizer at a loading complementary to the chromophore molar concentrations: PVK(49%)/C_{60}(1%)/BBP(50%$-x$%)/AODCST(x%) and PVK(49%)/C_{60}(1%)/BBP(50%$-x$%)/5CB(x%), where x was varied from 0% to 40%. Studying the chromophore concentration dependence of such composites where the chromophore is substituted with the plasticizer rather than just being added provides for consistent orientational effects since the glass transition temperature (T_g) was near room temperature of $\sim 21\,^{\circ}$C for all the concentrations. In particular, T_g of AODCST-containing plasticized composites remained constant within $1\,^{\circ}$C as x changed from 2% to 40% ($T_g \sim 20$ to $21\,^{\circ}$C), and glass transition temperature of 5CB-containing plasticized composites increased from $\sim 21\,^{\circ}$C at $x=5\%$ to $\sim 24\,^{\circ}$C at $x=40\%$. Thus orientational effects are similar for all the composites, as we proved by an orientational dynamics study using electric field induced second harmonic generation (EFISHG).[13] Also, the photoelectric properties of the materials connected to charge transport (mobility, trapping, and recombination rates) change with temperature relative to T_g, $\Delta T = T_{\mathrm{exp}} - T_g$, where T_{exp} is the temperature at which the experiment is conducted.[3,34,35] Therefore we ensured that ΔT is almost the same for all our composites. We used purified materials and freshly made samples for all our experiments since we found that both chemical impurities and sample aging over a period of several months led to deep trap formation, which would confound the data.

Sample preparation included the following steps. First, PVK was dissolved in a mixture of toluene and cyclohexanone wt. 4:1. Then, C_{60} was dissolved in toluene and added to a solution of PVK. Finally, the dye and the plasticizer were added to a solution of PVK and C_{60}. The volume concentration of C_{60} was calculated to be $N_A \approx 3.8\times 10^{24}\,\mathrm{m}^{-3}$. For mobility and photogeneration efficiency measurements, we prepared spin-coated samples on an Al substrate, while another Al electrode was deposited directly on top of the films. For photorefractive measurements we first prepared the films on the indium tin oxide (ITO) slides and then sandwiched them together and baked them in a vacuum oven at $120\,^{\circ}$C for 1 h.

The thickness of the samples for mobility and photogeneration efficiency measurements (Al electrodes) was $\sim$5–10 μm, and $\sim$30–70 μm for the photorefractive samples (ITO electrodes). We used both types of electrodes for dc photoconductivity measurements to ensure that the parameters calculated from the photocurrent transients are not influenced by the type of the electrode or sample thickness. The dielectric constant was measured at a frequency of 1 Hz using a capacitance bridge.

B. Photoconductive measurements

Equation (1) introduced in Sec. II is valid for the bulk material of infinite extent. In real experiments, the external circuit and electrodes may influence the observed behavior.[19,36,37] Because of the high degree of disorder and field dependence of all of the photoelectric parameters in polymers, a systematic analysis of current–voltage characteristics for different electrodes and their combinations is necessary to fully elucidate the electrical characteristics.[38–41]

Schildkraut and Cui[18] found good agreement between the steady state values for free carrier density, amplitude, and phase of space-charge field calculated from the bulk dynamic equations [e.g., Eq. (1)] for no boundary conditions (infinite bulk), ohmic boundary conditions (''infinite'' supply of charge from the electrodes), and blocking boundary conditions (Schottky barrier). We performed the dc photoconductivity experiments with two types of electrodes, Al and ITO, and for our experimental conditions (range of electric fields and intensities) did not find differences between the parameters calculated from the photocurrent transients. Thus we assume Eq. (1) approximates our samples well.

1. dc photoconductivity (short time scale)

For the short time scale measurements ($t < 50\tau_0$, where τ_0 is the average lifetime of a free carrier), we applied an electric field to the sample and waited until all the transient processes disappeared, then opened a shutter (switching time below 40 μs) and recorded the sample current under 633 nm illumination with an oscilloscope. For unplasticized composites the time span of this short time scale experiment was $\lesssim$4 s, while for the composites with plasticizer it was $\lesssim$40 s depending on the applied electric field. We performed this experiment for various electric fields and incident intensities. The photocurrent transients were then fit to a biexponential function

$$\rho_{\mathrm{fit}} = A[1 - Be^{-\lambda_{10}t} + (B-1)e^{-\lambda_{20}t}] \tag{14}$$

and the product of trapping rate and density of available shallow traps $\gamma_T M_{T1}$, the recombination rate γ, and the shallow trap detrapping rate β_1 were determined as functions of intensity and electric field in accordance with the procedure described in Sec. II A 1 *a*. From the electric field dependence of the trapping rate, we calculated the parameter β_γ [defined in Eq. (2)].

2. Dark conductivity and dc photoconductivity (long time scale)

For dark conductivity and the long time scale ($t > 10^3 \tau_0$) photoconductivity measurements, we monitored the current through the sample for ~20 min using a Keithley 6517 electrometer. A typical experimental run for plasticized samples included the following: the electric field was turned on, and the dark current (j_{dark}) was recorded for ~20 min. Then, the electric field was turned off and then in 2 min turned on again, and dark current was monitored again for ~20 min. If the first two dark current runs reproduced, then the light was turned on, and the current under illumination (j_{light}) was monitored for another ~20 min. Then, the photocurrent j_{photo} was calculated using $j_{\text{photo}} = j_{\text{light}} - j_{\text{dark}}$. If the first two dark current runs did not reproduce, a third dark current run was executed, and for all the samples under study the third run reproduced the second.

In unplasticized composites the dark current is due to injection from the electrodes. It reaches steady state in several seconds and is at least an order of magnitude smaller than the photocurrent at the incident intensity 20 mW/cm^2 at an applied field of $E_0 \sim 40\ \text{V}/\mu\text{m}$. In plasticized samples the dark current is due to both injection from the electrodes and to impurity ions moving towards opposite electrodes. It reaches a steady state only after 20–30 min and at low electric fields ($E_0 \sim 10\ \text{V}/\mu\text{m}$) is ~30% of the photocurrent at the incident intensity $I_0 \sim 40\ \text{mW/cm}^2$, so it is important to take careful measurements of dark current to reliably determine the photocurrent.[28]

The long time scale photoconductivity measurement was performed as a function of applied field and incident intensity. The photocurrent transients were fit to Eq. (14), and the product of trapping rate and density of available deep traps $\gamma_T M_{T2}$ and the detrapping rate β_2 for deep traps were determined as described in Sec. II A 1 *b*.

3. Mobility

Mobility was measured using the time-of-flight (TOF) technique. We used a wavelength of 320 nm that is the third anti-Stokes of H_2—stimulated Raman-shifted 532 nm of a Nd:YAG laser with a 3.5 ns pulse of ~5 μJ/pulse. The sample current was transformed to a voltage, amplified, and monitored with an oscilloscope. Then, mobility was calculated using a log-log plot for determining a transient time t_T and the relation $\mu = d^2/(t_T V)$, where d is the thickness of the sample and V is the voltage applied. We measured mobility as a function of electric field to determine the parameter β_μ defined in Eq. (2) that describes the mobility field dependence. For unplasticized samples and plasticized samples with low chromophore content (<10% concentration) the TOF transients could be easily resolved at electric fields $E > 20\ \text{V}/\mu\text{m}$. The transients for high chromophore content plasticized samples (>10% chromophore concentration) at all electric fields and low chromophore content plasticized samples at electric fields $E < 10\ \text{V}/\mu\text{m}$ yielded TOF transients that were too dispersive for reliable determination of the mobility from TOF experiment. In this case we estimated the mobility from the dc photoconductivity measurements using the formula[4] $\mu = d^2(\gamma_T M_{T1})/(2\ \text{V})$. This estimate showed reasonable agreement with TOF results for unplasticized and low chromophore content plasticized samples at higher electric fields ($E > 20\ \text{V}/\mu\text{m}$), thus we used it to calculate the mobility for the samples which could not be accurately measured by the TOF technique.

4. Photogeneration efficiency

The xerographic discharge technique was used for this measurement for unplasticized samples and plasticized samples at higher electric fields ($E > 20\ \text{V}/\mu\text{m}$). The sample was charged to an initial voltage and then disconnected from the power supply. The decay under HeNe illumination of 633 nm was monitored using a static voltmeter and an oscilloscope. The cross section of photogeneration s was calculated from the slope of the discharge rate versus illumination intensity: $|(dV/dt)|_{\text{light}} = [sd^2 eN_A/(\epsilon_0 \epsilon)]I_0$, where I_0 is the intensity of light, d is a thickness of the sample, ϵ is a dielectric constant, and N_A is a number density of C_{60}. We also estimated the photogeneration cross section from the dc photoconductivity as described in Ref. 4 using the formula $s = (\overline{\rho_0}\gamma_T M_{T1})/(I_0 N_A)$ where $\overline{\rho_0}$ is the maximum free charge density. We ensured consistency of this method by comparing the photogeneration cross sections determined from dc photoconductivity and xerographic discharge for unplasticized and plasticized samples at higher fields where the xerographic discharge technique provided reliable data. For plasticized samples at low electric fields ($E < 10\ \text{V}/\mu\text{m}$) reliable measurements of xerographic discharge could not be obtained because of relatively large dark current. In this case, we calculated the photogeneration cross section s from the dc photoconductivity. Analyzing the electric field dependence of s, we obtained the photogeneration field-dependence parameter p of Eq. (2) for each composite.

C. Photorefractive measurements

The diffraction efficiency was measured in a degenerate four-wave mixing geometry. The grating was written with two *s*-polarized HeNe 633 nm beams of the same internal intensity with a total intensity varying from 25 to 400 mW/cm^2. The probe beam was *p*-polarized with intensity 5 mW/cm^2. The external angle between the crossing beams was 28°, and the external angle between the sample normal and the bisector of two writing beams was 50°. This experimental geometry along with the index of refraction $n = 1.63$[7] yielded a diffraction grating of period $\Lambda \approx 1.8\ \mu$m. A typical experiment for unplasticized samples included the following steps: first, we applied the electric field (~30 V/μm) with one writing beam and the probe beam on, then in 10 s when all the transients disappear, we opened the other writing beam with a shutter and recorded the diffracted signal with a photodetector, lock-in amplifier, and computer. After the diffracted signal reached the quasi-steady state (~20 s), the light was blocked and the field was turned off. The samples were kept in the dark for ~30 min before the next measurement to assure complete decay of the space charge field and the absence of ionized acceptors and filled traps. For plasticized samples, the experimental run was similar, with the

TABLE I. Photoelectric parameters relevant for photorefraction for composites 1–4. No plasticizers were added.

Composite	s, 10^{-5} m^2/J	μ, 10^{-11} $m^2/(V\,s)$	$\gamma_T M_{T1}$, s^{-1}	$\gamma_T M_{T2}$, s^{-1}	β_1, s^{-1}	β_2, s^{-1}	γ, 10^{-19} m^3/s	β_μ, 10^{-4} $(m/V)^{1/2}$	β_γ, 10^{-4} $(m/V)^{1/2}$	p	ϵ
1 Neat	1.7	5.3	850		2.7		2.5	4.9±0.2	8.3±0.5	2.04±0.06	3.1
2 AODCST	1.6	3.9	300	3	0.75	8.5×10^{-4}	0.09	5.8±0.5	3.3±0.4	2.04±0.04	4.3
3 PDCST	0.84	2.5	770	23	0.3	1.5×10^{-4}	0.08	4.9±0.2	6.5±0.3	2.04±0.04	3.8
4 5CB	0.83	1.7	550		1.5		0.09	6.0±0.3	4.6±2.0	2.1±0.2	4.5

difference being that we used a lower electric field ($\sim$10 V/μm) and waited for at least 60 s after turning the electric field on to ensure that most of the impurity ions have accumulated at the electrodes.[42] Also, for plasticized samples, we monitored the diffracted signal following homogeneous illumination of various durations (up to 1 h) to study the influence of deep traps on the photorefractive signal for different chromophores and chromophore concentrations.

We fit the PR grating formation dynamics with a biexponential

$$\eta = \eta_0[1 - ae^{-\nu_1 t} - (1-a)e^{-\nu_2 t}]^2. \quad (15)$$

In unplasticized composites the faster speed ν_1 was attributed to photoconductivity and dominated with weight $a \approx 0.7$ to 0.8 (inset of Fig. 7). The slower speed ν_2 in these composites is due to orientational enhancement which was verified experimentally by comparing the ratio of p-polarized and s-polarized diffraction efficiencies η_p/η_s to this ratio calculated from geometry of the experiment and the electro-optic effect.[43] The slower speed was intensity independent and on the order of 0.5–1 s^{-1}, which is consistent with our EFISHG measurements of the dynamics of chromophore reorientation in these unplasticized materials.[13]

In plasticized composites, both the faster (ν_1) and slower (ν_2) speeds were attributed to photoconductivity and varied from 0.1 to 10 s^{-1} and from 0.01 to 1 s^{-1}, respectively, depending on the chromophore concentration, applied electric field, and incident light intensity. Thus the chromophore reorientation time constant of about 50 ms (as determined by EFISHG) which is faster than both ν_1 and ν_2 does not contribute.

IV. RESULTS

A. Unplasticized composites

In this section we determine the photoconductivity parameters for composites 1–4 and discuss the differences in the parameters depending on the chromophores. Then based on these parameters we model the dynamics of photorefractive grating formation and compare it to experiment.

1. Photoelectric properties

The photoconductivity parameters and rates introduced in Sec. II and calculated from the TOF, xerographic discharge, and dc photoconductivity (at incident intensity $I_0 = 100\,mW/cm^2$) experiments described in Sec. III at the electric field $E_0 = 40\,V/\mu m$ are summarized in Table I. All the trends we describe in this section are applicable for composites 1–4 in the studied electric field range of $E \approx 20$–$80\,V/\mu m$. Diagrams describing charge generation, transport, and trapping for different composites are shown in Fig. 6. Here we used the relative highest occupied molecular orbital (HOMO) level energies for PVK (0 eV), C_{60} (−0.17 eV), AODCST (0.03 eV), PDCST (0.1 eV), and 5CB (<-0.4 eV) provided in Ref. 8.

Photogeneration cross-section s is a measure of quantum efficiency and for low absorption is given by the relation $s = \alpha\phi/(\hbar\omega N_A)$ where α is the absorption coefficient, ϕ quantum efficiency, and ω is the light frequency. Photogeneration cross section microscopically depends on the donor–acceptor charge transfer and electron–hole dissociation rates.[44] According to their HOMO levels, chromophores AODCST and PDCST as well as PVK are donors with respect to C_{60}, and thus could participate in photogeneration. If we take into account the dependence of the charge transfer rate k_{CT} on the energy difference ΔE_{DA} between HOMO levels of donor and acceptor[44,45] $k_{CT} \sim \exp[-(\Delta E_{DA} - \lambda)^2/(4\lambda k_B T)]$ where λ is the reorganization energy, then in the noninverted regime, the photogeneration efficiency would be highest for composite 3, followed by composites 2, 1, and 4. The noninverted regime refers to the case $\Delta E_{DA} < \lambda$, which seems to describe our composites.[44] However, the donor–acceptor charge transfer is not the only factor that contributes to charge generation. The other factor is the electron–hole dissociation,[44] which proceeds more strongly as the mobility increases. Based on our results for photogeneration cross sections and mobilities for composites 1–4 (Table I), we conclude that the mobility differences that affect dissociation in addition to the charge transfer rate k_{CT} could account for the differences in quantum efficiencies for the composites 1–4.

The hole mobility of all of the composites 2–4 is smaller than that for the PVK/C_{60} (composite 1). This is expected when adding polar chromophores to the system due to the

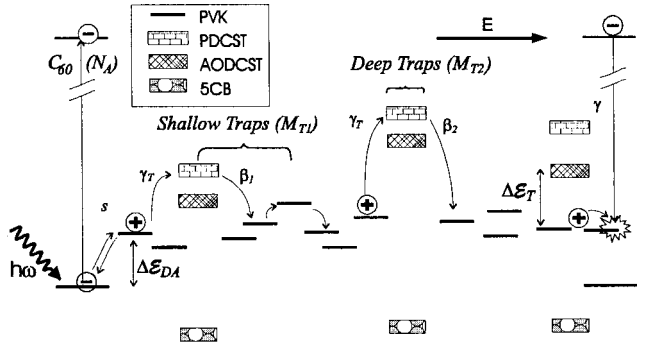

FIG. 6. Schematic representation of the intrinsic states and processes of a PR composite with various chromophores.

increase in energetic disorder.[20,46] Based only on the dipole moment of the chromophore, composites 2 and 3 would be expected to yield similar mobilities due to almost equal dipole moments (6.9 D for AODCST and 6.6 D for PDCST), and composite 4 would yield the higher mobility than the composites 2 or 3 since the dipole moment of 5CB (4.1 D) is lower than that of both AODCST and PDCST. Our results show that the composite 2 possesses the largest value for mobility out of three composites with chromophores (2–4). We attribute this to the fact that the HOMO level of AODCST is situated inside the transport manifold of PVK, so that AODCST molecules participate in transport by increasing the density of transport states.

All three chromophores influence the PVK/C_{60} system modifying the position and depth of shallow traps that are intrinsic to PVK.[3] Here we need to make a distinction between shallow traps whose release (detrapping) time is much smaller than the transit time, in other words shallow traps that broaden the tail of the current transients observed in our TOF experiment, and traps whose release time is much larger than the transit time. The latter traps are relevant for photorefractive performance of the polymer composites considered here.

The parameters describing shallow traps are the trapping rate γ_T, the total number density of available shallow traps M_{T1}, and the detrapping (releasing) rate β_1. Comparing detrapping rates β_1 for composites 1–4 (Table I), we observe that the addition of all chromophores leads to a decrease in detrapping rate β_1 that may arise from a decrease in the overlap integral (intersite distance), an increase in the trap energy depth ΔE_T (Fig. 6),[24,47] or both. Both AODCST and PDCST have a larger impact on β_1 than 5CB since they can provide sites that can serve as deeper traps. Since in our experiments we cannot measure the trapping rate γ_T and total trap density M_{T1}, but only the product $\gamma_T M_{T1}$, we can only speculate about possible contributions of each. The trapping rate γ_T at a given electric field is expected to depend on the free hole mobility and the neutral trap capture cross section.[24] In this case we should expect a smaller trapping rate γ_T value for the composites 2–4 in comparison to composite 1 due to decreased mobility. In composite 3 the product $\gamma_T M_{T1}$ is larger than that of composites 2 and 4 which could indicate that PDCST actually adds shallow traps to the system in addition to just changing the average depth of existing shallow traps in pure PVK. On the contrary, composite 2 has the smallest product $\gamma_T M_{T1}$ which could mean that AODCST reduces the relative density of relevant shallow traps intrinsic to PVK by providing extra transport sites. Similar to shallow traps, we characterize deep traps by their number density M_{T2} and detrapping rate β_2. We could not detect deep traps in the PVK/C_{60} system and in composite 4 (with 5CB as chromophore) which means that the density of available deep traps (M_{T2}) in these composites is on the order of 1% or less of the acceptor density N_A. Both AODCST (composite 2) and PDCST (composite 3) create deep traps, with the trap depth larger for PDCST than for AODCST which is consistent with experimental studies performed with these chromophores in Ref. 8 and with our numerical simulations. From the comparison between $\gamma_T M_{T2}$ values for composites 2 and 3 we conclude that PDCST creates more deep traps than AODCST as would be expected by their HOMO levels.

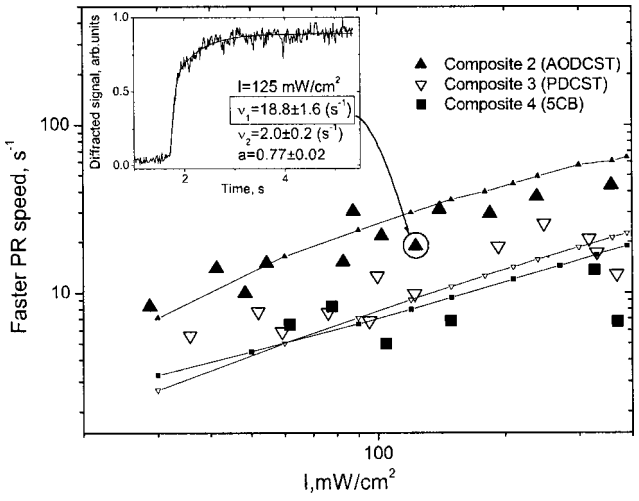

FIG. 7. Photorefractive speed as a function of intensity for composites 2–4: line with symbols represents a theoretically predicted speed for this composite (no adjustable parameters) using Eqs. (11)–(13); symbols represent actual PR speed determined from the FWM experiment. The inset shows a typical transient measured in composite 2 at a total intensity of 125 mW/cm^2.

The recombination rate γ describes interaction of the free hole with the ionized acceptor (C_{60}^-) and usually is treated as Langevin bimolecular recombination $\gamma = e\mu/(\epsilon\epsilon_0)$.[24] According to this relation, the ratio γ/μ depends only on dielectric constant ϵ of the material. In polymers, due to disorder, deviations from the Langevin form are observed.[24] Our measured recombination rate for PVK/C_{60} shows good agreement with the value obtained using the Langevin form. However, the measured values for composites 2–4 are considerably lower than the corresponding values calculated from the Langevin form.

2. Photorefractive properties

In this section we applied all the photoelectric parameters we determined above to Eq. (11). When considering the space-charge field formation, we used the values for mobility, trapping, and recombination rates calculated using the value of the projection of the electric field on grating vector while the photogeneration cross section was calculated using the applied electric field. We solved Eq. (11) to determine the dynamics of photorefractive grating formation $[E_1(t)]$ for the composites 2–4. Then, we calculated the diffraction efficiency signal time evolution as it appears in the four wave mixing (FWM) experiment[48] $\eta \sim E_1(t)^2$ and fit with the function of Eq. (13) to predict the photoconductive part of photorefractive speed ν. The calculated speed ν is to be compared with the measured ν_1 introduced in Sec. III C. The anticipated speed ν as a function of total internal intensity of two beams for the composites 2–4 is shown in Fig. 7 (lines with symbols). The measured (as described in Sec. III C) faster component of the photorefractive speed ν_1 for composites 2–4 is also shown in Fig. 7 (symbols) and is in a reasonable agreement with the speed ν predicted using ex-

perimentally determined photoelectric parameters for these composites. Both calculated and experimentally measured PR speed are sublinear functions of light intensity (ν, $\nu_1 \sim I^a$, where $a=0.6$ to 0.7 depending on a composite), similar to intensity dependencies of simulated and measured photoconductivity (taken at maximal photocurrent value, see Fig. 2) in these composites.

B. Plasticized composites

In this section we consider the dependence of the PR properties of composites on the chromophore and plasticizer concentration. First, we consider how substitution of the chromophore molecule by the plasticizer [increase in parameter $x(\%)$ introduced in Sec. III A] affects the photoelectric parameters such as mobility, photogeneration efficiency, recombination, trapping, and detrapping rates. We studied this for two chromophores, 5CB and AODCST, to determine the influence of the chromophore ionization potential on these characteristics. Second, we used the parameters determined from photoconductivity to model the time evolution of a photorefractive grating (diffracted signal observed in FWM experiment) and compare it with experimental data for different concentrations. Finally, we discuss the dependence of the diffracted signal on the illumination history for different concentrations of AODCST and 5CB.

1. Photoelectric properties

The most distinct feature of the plasticized composites in comparison to unplasticized ones is the presence of large dark current observed in ''fresh'' samples that were not exposed to either electric field or illumination. In this case the dark current is caused by both charge injection from the electrodes and native ionic impurities[49] that become mobile under the electric field due to the conformational freedom of the plasticized polymer chains.[24] As the sample is kept under electric field, the mobile ions move towards the oppositely charged electrodes and either neutralize[42] or build up, reducing the electric field inside the polymeric film. The samples of all concentrations x for both 5CB and AODCST showed similar behavior. After the transient, the current gradually decreases until it reaches a quasi-steady level, which in our materials occurs at time $\sim$20–30 min after the electric field is turned on.[28] We performed all the measurements after the samples were electrically cleansed to avoid dynamic effects directly induced by moving impurity ions. Although we tried to maintain exactly the same experimental conditions for the samples at all concentrations, our measurements of both photoconductivity and diffraction efficiency at different times after turning on the electric field without any prior illumination show that internal electric fields are different for different concentrations of the chromophore. However, these effects were minor in comparison with the direct concentration effects that we investigated. The energy diagram illustrating different composites studied is shown in Fig. 8. Based on the ionization potentials of the plasticizer and chromophores, we expect that an increase in concentration of 5CB (relative to the concentration of plasticizer BBP) should not change the mobility, photogeneration efficiency, trapping, and other photoelectric parameters for reasons other than an increase in energetic disorder due to the difference in dipole moments of 5CB ($4.1D$) and BBP ($1.1D$). In the case of AODCST, however, in addition to the change in energetic disorder, we also expect changes due to the contribution of AODCST sites in charge photogeneration and transport. Indeed, our results show that both mobility and photogeneration cross section increase with concentration of AODCST and stay almost constant for all concentrations of 5CB. Although these trends were observed for the whole range of electric fields studied (1–50 V/μm), the most pronounced concentration dependence was found at low electric fields ($<$15 V/μm). This could be due to the smaller influence of energetic disorder at low fields, so that the largest impact on concentration dependence is attributed to the effects only due to ionization potential of the chromophores relative to transport states. The concentration dependence of mobility and photogeneration cross section for 5CB and AODCST at electric field $E_0 = 10\,\mathrm{V}/\mu\mathrm{m}$ is shown in Fig. 9. As determined from dc photoconductivity at electric field $E_0 = 10\,\mathrm{V}/\mu\mathrm{m}$ and intensity $I_0 = 40\,\mathrm{mW/cm^2}$, the product $\gamma_T M_{T1}$ increased monotonically in a similar to s and μ manner from 3.5 s^{-1} for $x = 0\%$ [PVK(49%)/BBP(50%)/C_{60}(1%)] to 20 s^{-1} for $x = 40\%$ in the case of AODCST and did not change in the case of 5CB. This change reflects the increase in mobility and intersite distance that affect the trapping rate for AODCST and no changes in these for 5CB.[28] The detrapping rate β_1 increased from $\sim$0.05 to $\sim$0.1 s^{-1} for AODCST, reflecting increase in the overlap integral (decrease in intersite distance). The recombination rate was $\sim 2\times10^{-21}\,\mathrm{m^3/s}$ and did not change appreciably with concentration, probably because the increase in mobility in the case of AODCST was partially compensated by an increase in dielectric constant as the concentration of AODCST increased.

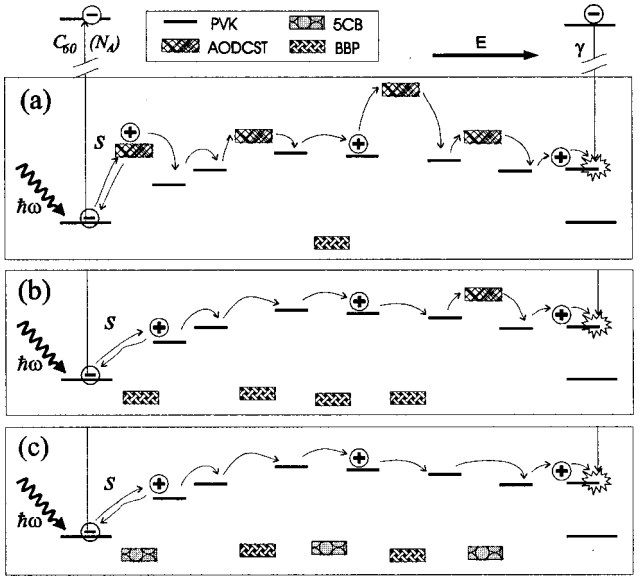

FIG. 8. Illustration of chromophore and plasticizer roles in charge generation, transport, and trapping: (a) high x%, AODCST; (b) low x%, AODCST; and (c) any x%, 5CB.

The presence of deep traps in the composites was studied by monitoring dc photoconductivity on a long time scale (Sec. II A 1 b).[28] The composites with $x=0$ and with any

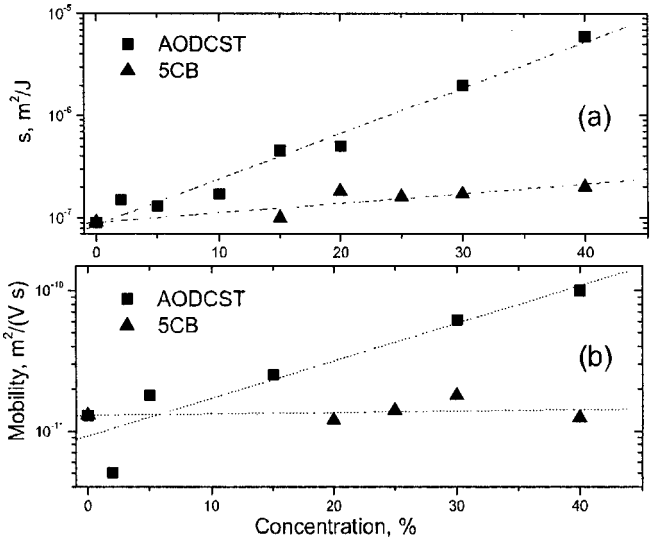

FIG. 9. Concentration dependence of (a) photogeneration cross section and (b) mobility. The lines provide visual guidance.

concentration of 5CB showed no photodegradation and thus the deep trap density in these composites was below our detection limit of $M_{T2} \leqslant 0.01 N_A$. Our numerical simulations of PR dynamics show that when the available density of deep traps is on the level $M_{T2} \sim 0.01 N_A$ or less (provided shallow trap-unlimited regime $M_{T1} \gg N_A$), the PR grating time evolution is not influenced by deep traps. In the AODCST-containing composites, the degradation of the photocurrent increased as the concentration of AODCST increased, so that the product $\gamma_T M_{T2}$ describing deep trapping increased from $\sim 0.02\ \mathrm{s}^{-1}$ for $x=2\%$ to $\sim 1.6\ \mathrm{s}^{-1}$ for $x=40\%$, and the detrapping rate β_2 correspondingly changed from 1.1×10^{-5} to $8.2\times10^{-4}\ \mathrm{s}^{-1}$, although the values for low concentrations of the chromophore may contain a large error due to the small concentration of deep traps M_{T2} in these composites. Similar to the method described in Sec. IV A 2, we substitute all the calculated values into the equations describing photorefractive grating formation [Eq. (11)] and model the PR performance of the composites. We fit the calculated diffraction efficiency $\eta(t)$ with a biexponential function [Eq. (15)] since, as we mentioned above for these samples, both the slow and fast components of the photorefractive speed are due to photoconductivity. The calculated faster and slower PR speed (ν_1 and ν_2, respectively) as a function of concentration of the chromophore with no adjustable parameters is presented in Fig. 10(a) (line with symbols corresponding to concentrations for which we determined photoelectric parameters on whose basis the PR speed was calculated).

2. Photorefractive properties

The faster and slower PR speed (ν_1 and ν_2) obtained from the biexponential fit of Eq. (15) to the experimentally measured diffraction efficiency for different concentrations is plotted in Fig. 10(a) (symbols) along with a characteristic fit [Fig. 10(b)]. Faster PR speed in both 5CB and AODCST-containing composites shows reasonable agreement with the values of ν_1 calculated from photoconductivity (line with

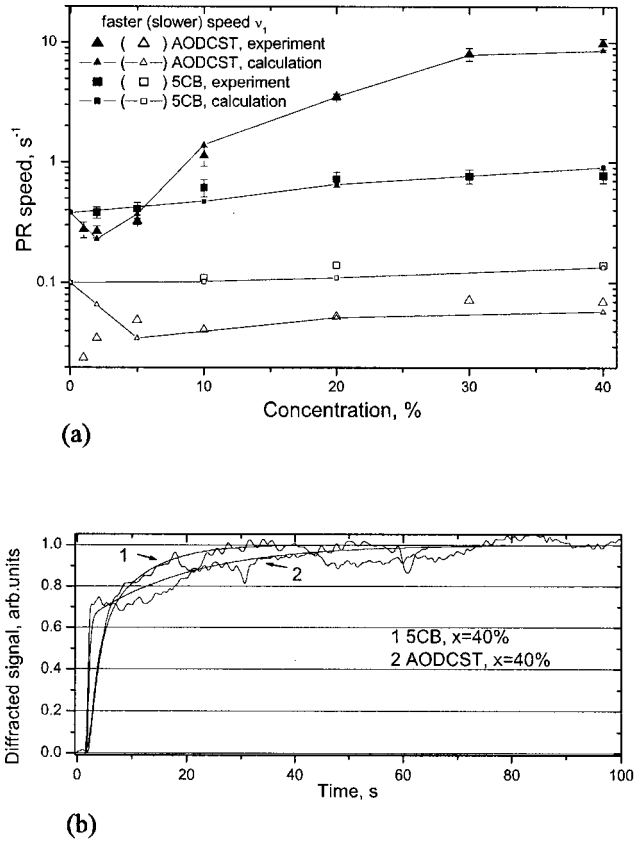

FIG. 10. (a) Concentration dependence of faster and slower PR speed for 5CB- and AODCST-containing composites. Lines with symbols correspond to the photoelectric parameter values for PR speed calculated using Eqs. (11), (12), and (15); symbols correspond to FWM experimental data at applied field $E_a = 10\ \mathrm{V}/\mu\mathrm{m}$ and total internal intensity $I = 300\ \mathrm{mW/cm^2}$. (b) Data and fit with Eq. (15) to two composites.

symbols). The experimentally measured slower speed ν_2 shows good agreement with calculated values for 5CB-containing composites. Although we could not find monotonic dependence of slower PR speed on various parameters, our simulations show that at low photogeneration efficiencies and charge carrier mobilities electric field dependence of photoelectric rates (i.e., nonzero parameters p, β_μ, β_γ) leads to nonsingle exponential behavior of space-charge field in materials without deep traps, such as our 5CB-containing composites.

In materials with deep traps, the slower component is influenced by trapping rate γ_T, deep trap density M_{T2}, and detrapping rate β_2. The slower PR speed in AODCST-containing composites shown in Fig. 10(a) is calculated using shallow and deep trap unlimited approximation (*Case 3*). As seen from Fig. 10(a), *Case 3* describes well composites with high chromophore content. However, at low chromophore concentrations, it seems that the deep trap limited *Case 2* needs to be considered.[27,28] In these materials, it is not enough to know the trapping parameter $\gamma_T M_{T2}$ that we are able to determine from the photoconductivity, but knowledge of the trapping rate γ_T and trap density M_{T2} separately is required to predict the slower PR speed.

According to our simulations, the materials with deep traps are expected to show a change in both rise and decay

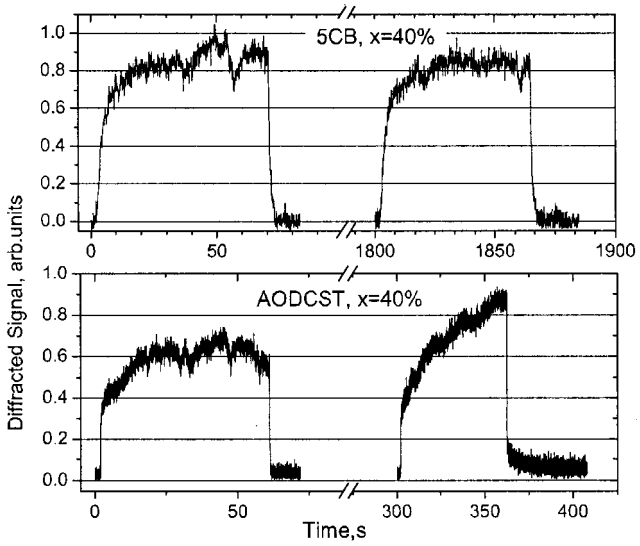

FIG. 11. Influence of homogeneous illumination prior to FWM experiment on diffracted signals for (a) $x=40\%$, 5CB and (b) $x=40\%$, AODCST at applied electric field $E_a=10\ \mathrm{V}/\mu\mathrm{m}$ and total incident intensity $I_0=300\ \mathrm{mW/cm^2}$.

transients due to the duration of uniform illumination prior to the experiment, which is supported by our experimental data. Figure 11 illustrates the diffraction efficiency time evolution in ''fresh'' samples and preilluminated samples of the composites containing $x=40\%$ of 5CB [Fig. 11(a)] and $x=40\%$ of AODCST [Fig. 11(b)]. The experimental run consisted of the following steps. First, the electric field of 10 $\mathrm{V}/\mu\mathrm{m}$ was turned on and kept on for 60 min without any illumination. Then, one of the writing beams of intensity 150 $\mathrm{mW/cm^2}$ was turned on, and then after $\sim$20 s the second writing beam of the same intensity was turned on, and the diffraction grating formation was monitored for 60 s. Then, one writing beam was turned off, and the grating decay was monitored. The second writing beam (with the applied field on) was illuminating the sample for 5–15 min, and then again the second beam was turned on and grating formation monitored. To ensure that the effects we observe in this experiment are due to illumination and not due to internal fields formed by uncompensated traps and impurity ions, we performed a similar experiment but without any illumination between the grating decay and formation measurements. Our results show that all the dependencies described here and shown in Fig. 11 are due to illumination only. The 5CB-containing composite showed no substantial history dependence because the dynamics involves only shallow traps, and the equilibrium between photogeneration, trapping, detrapping, and recombination processes in the system is reached within several seconds and then does not change over a long time scale. In such systems, the long time scale illumination does not change the density of ionized acceptors and filled traps, and so the initial conditions for the onset of diffraction are the same at any time. Thus there is no illumination history dependence (Fig. 11). The behavior is different for the composites with high AODCST concentration. After the sample illuminated for 5 min, the grating formation and decay are substantially different in comparison with those observed in the fresh sample. This is because after illumination the initial conditions for the grating formation change dramatically due to deep trap filling and ionized acceptor growth, so that deep traps noticeably contribute to the grating dynamics, as predicted by numerical simulations.[27,28]

The illumination history dependence can be undesirable for applications requiring a long time period grating formation/decay repetition in the presence of illumination and, thus materials containing deep traps are not suitable for these applications.

V. CONCLUDING REMARKS

We have carried out a detailed investigation of the processes that affect the PR speed. Although it has been previously experimentally demonstrated that photogeneration cross section and mobility have a large impact on PR speed, our calculations confirm this. However, we also demonstrate the role of other parameters such as recombination rate, trapping rate, and density of traps. We have shown the subtle role that traps play in photorefractive dynamics. We have also shown how the PR dynamics have a rather complicated form, but have nonetheless demonstrated how biexponential fits to the data can be useful when carried out over the appropriate time scales.

We considered two kinds of thermally accessible traps, shallow and deep. We attribute the shallow traps to structural defects and conformational traps of the carbazole units[50] in the photoconductor itself (PVK), which can be affected by the presence of chromophores. Although there could be some deep traps in PVK itself, the essential contribution in the density of deep traps that may affect the space-charge field formation is determined by the chromophores. Deep traps lead to slow growth of ionized acceptor density, as previously observed,[8] which leads to complicated long time scale PR dynamics and illumination history dependence of both photoconductive and photorefractive properties.

Ionized acceptor density (N_{A0}^i) was identified earlier in the literature[8,22] as ''deep photoexcitable photorefractive trap density,'' since it turned out to be approximately equal to *filled* trap density ($M_{10}+M_{20}$) measured in the two-beam coupling experiment.[8] We believe that photorefractive traps in polymer composites are not photoexcitable and are the ones we discussed above, which are due to structural defects in PVK and to the position of the ionization potential of a chromophore with respect to the photoconductor. The density of such traps in the material and their depth, together with other photoelectric rates intrinsic to the material, determines the dynamics of growth of the ionized acceptors. However, ionized acceptor density is indeed a good measure for filled trap density, since the relation $N_{AO}^i \approx M_{10}+M_{20}$ is always true according to the charge neutrality equation [last equation in Eq. (5)] under the condition of free charge density (ρ_0) much smaller than filled trap densities ($M_{10,20}$), which seems to be the case in most PR polymer composites. For example, if the same material is sensitized with different sensitizers (meaning that the photogeneration cross section s is the only parameter that changes in the system), the different filled trap densities (as manifested through different gain coefficients)

observed in the two-beam coupling experiment[30] are due to the difference in charge photogeneration efficiency, which leads to the difference in ionized acceptor density and, therefore, filled trap density.

Experimentally, we studied a set of unplasticized composites with 5CB, AODCST, and PDCST as chromophores and chromophore concentration dependence of plasticized composites with 5CB and AODCST as chromophores. We applied the modified Schildkraut and Buettner's model to compare both photoconductive and photorefractive properties of the composites under investigation. We were able to predict *with no adjustable parameters* the faster photorefractive speed for a variety of composites from the experimentally measured values of the relevant photoelectric rates. The slower PR dynamics was predicted *with no adjustable parameters* for composites with no deep traps (composites with 5CB as a chromophore) and with a high concentration of deep traps (high AODCST content composites). We also studied the influence of deep traps on the illumination history dependence of the photorefractive performance. The modified model seems to describe qualitatively the experimentally observed trends.

Figure 10 points out the complexities of assessing photorefractive speed and designing high speed materials. As can be seen in that figure, the slow time constant in AODCST composites is always slower than that for 5CB composites due to more deep trapping, while the fast time constant for AODCST composites can be faster than 5CB composites due to a higher density of states created by AODCST states within the transport manifold. The complete fit in Fig. 10(b) indicates the difficulties in assessing the PR speed. Diffraction builds more quickly in AODCST composites, but stabilizes more slowly compared with 5CB composites. An optimum chromophore would possess a fast component like the AODCST composite, but suppress a slow component like the 5CB composite. Such a chromophore would possess an ionization potential high enough and/or a density of states narrow enough so that deep traps are not formed even at high concentration to suppress the long time constant, but an ionization potential low enough so that its density of states overlaps with the transport manifold increasing the initial speed of grating formation. The ionization potential of 5CB is too high for this, while that of AODCST may be too low to avoid deep trapping. We are not aware of an optimized composite that exhibits both a fast short time constant and a short or suppressed long time constant. As is well-known, the presence of deeper traps slows the dynamics, but increases the diffraction efficiency. This trade-off must also be addressed depending on the requirements of the application. We believe that this study provides a method to assess the impact of trapping on dynamics in a quantitative manner.

Despite some successful predictions we were able to make using the modified model, there are some outstanding issues. First of all, the composites with trap densities on the level of $M_T \sim 0.01-1 N_A$ cannot be treated the way elaborated for the case $M_{T1,2} \gg N_A$, and thus in many composites the longer scale behavior of space-charge field cannot be predicted as well as the shorter time scale behavior. Second, the trapping, detrapping, and recombination rates (γ_T, β, γ) were found to depend sublinearly on light intensity[28] which is not explicitly included or predicted by the model, thus it seems that some process has not been taken into account. Third, it might be helpful to include the effect of the formation of the internal electric field inside the sample due to the filling of uncompensated traps as well as non-neutralized impurity ions. Also, both photoconductivity and photorefractive signals are sensitive to the presence of deep traps in the composite, so that impurities that could serve as deep traps can obscure the performance of a purer system. A final remark is that Eq. (1) is written for an infinite bulk material and does not take into account the possible effects of electrodes. These issues require further study.

ACKNOWLEDGMENTS

The authors thank Professor R. Twieg for AODCST. Dr. V. Ostroverkhov is acknowledged for assistance in the numerical simulations. Dr. I. Shiyanovskaya and Dr. J. Andrews are acknowledged for helpful discussions. The research described in this article was made possible by the support of the National Science Foundation through the ALCOM Science and Technology Center (DMR 89-20147), and by the Air Force Office of Scientific Research, Air Force Material Command, USAF (F49620-99-1-0018).

[1] J. C. Scott, L. T. Pautmeier, and W. E. Moerner, J. Opt. Soc. Am. B **9**, 2059 (1992).
[2] S. Schloter, A. Schreiber, M. Grasruck, A. Leopold, M. Kol'chenko, J. Pan, C. Hohle, P. Strohriegl, S. J. Zilker, and D. Haarer, Appl. Phys. B: Lasers Opt. **68**, 899 (1999).
[3] T. K. Daubler, R. Bittner, K. Meerholz, V. Cimrova, and D. Neher, Phys. Rev. B **61**, 13515 (2000).
[4] E. Hendrickx, Y. Zhang, K. B. Ferrio, J. A. Herlocker, J. Anderson, N. R. Armstrong, E. A. Mash, A. Persoons, N. Peyghambarian, and B. Kippelen, J. Mater. Chem. **9**, 2251 (1999).
[5] M. Grasruck, A. Schreiber, U. Hofmann, S. J. Zilker, A. Leopold, S. Schloter, C. Hohle, P. Strohriegl, and D. Haarer, Phys. Rev. B **60**, 16543 (1999).
[6] S. J. Zilker *et al.*, Chem. Phys. Lett. **306**, 285 (1999).
[7] A. Grunnet-Jepsen, C. L. Thompson, and W. E. Moerner, J. Opt. Soc. Am. B **15**, 905 (1998).
[8] A. Grunnet-Jepsen, D. Wright, B. Smith, M. S. Bratcher, M. S. DeClue, J. S. Siegel, and W. E. Moerner, Chem. Phys. Lett. **291**, 553 (1998).
[9] B. Kippelen, Sandalphon, K. Meerholz, and N. Peyghambarian, Appl. Phys. Lett. **68**, 1748 (1996).
[10] K. Hoechstetter, S. Schloter, U. Hoffmann, and D. Haarer, J. Chem. Phys. **110**, 4944 (1998).
[11] E. Mecher, C. Brauchle, H. H. Horhold, J. C. Hummelen, and K. Meerholz, Phys. Chem. Chem. Phys. **1**, 1749 (1999).
[12] K. S. West, D. P. West, M. D. Rahn, J. D. Shakos, F. A. Wade, K. Khand, and T. A. King, J. Appl. Phys. **84**, 5893 (1998).
[13] O. Ostroverkhova, A. Stickrath, and K. D. Singer, J. Appl. Phys. **91**, 9481 (2002).
[14] D. Wright, M. A. Diaz-Garcia, J. D. Casperson, M. DeClue, W. E. Moerner, and R. J. Twieg, Appl. Phys. Lett. **73**, 1490 (1998).
[15] G. Bauml, S. Schloter, U. Hoffmann, and D. Haarer, Opt. Commun. **154**, 75 (1998).
[16] J. S. Schildkraut and A. V. Buettner, J. Appl. Phys. **72**, 1888 (1992).
[17] B. Yuan, X. Sun, C. Hou, Y. Li, Z. Zhou, Y. Jiang, and C. Li, J. Appl. Phys. **88**, 5562 (2000).
[18] J. Schildkraut and Y. Cui, J. Appl. Phys. **72**, 5055 (1992).
[19] J. Mort and D. Pai, *Photoconductivity and Related Phenomena* (Elsevier, New York, 1976).
[20] A. Goonesekera and S. Ducharme, J. Appl. Phys. **85**, 6506 (1999).
[21] Y. Cui, B. Swedek, N. Cheng, J. Zieba, and P. N. Prasad, J. Appl. Phys. **85**, 38 (1999).

[22] J. A. Herlocker, C. Fuentes-Hernandez, K. B. Ferrio, E. Hendrickx, P.-A. Blanche, N. Peyghambarian, and B. Kippelen, Appl. Phys. Lett. **77**, 2292 (2000).
[23] N. V. Kukhtarev, V. B. Markov, M. Soskin, and V. L. Vinetskii, Ferroelectrics **22**, 961 (1979).
[24] M. Pope and C. Swenberg, *Electronic Processes in Organic Crystals and Polymers* (Oxford University, New York, 1999).
[25] B. Movaghar, Philos. Mag. B **65**, 811 (1992).
[26] K. Meerholz, E. Mecher, R. Bittner, and Y. Nardin, J. Opt. Soc. Am. B **15**, 2114 (1998).
[27] O. Ostroverkhova and K. D. Singer, Proc. SPIE **4462**, 163 (2001).
[28] O. Ostroverkhova, Ph.D. thesis, Case Western Reserve University, 2001.
[29] *Photorefractive Materials and Their Applications I*, edited by P. Gunter and J.-P. Huignard (Springer-Verlag, Berlin, 1988).
[30] O. Ostroverkhova, U. Gubler, D. Wright, W. E. Moerner, M. He, A. Sastre-Santos, and R. Twieg, Adv. Fun. Mat. (to be published).
[31] S. M. Silence, G. C. Bjorklund, and W. E. Moerner, Opt. Lett. **19**, 1822 (1994).
[32] J. A. Herlocker, K. B. Ferrio, E. Hendrickx, B. D. Guenther, S. Mery, B. Kippelen, and N. Peyghambarian, Appl. Phys. Lett. **74**, 2253 (1999).
[33] M. A. Diaz-Garcia, D. Wright, J. D. Casperson, B. Smith, E. Glazer, W. E. Moerner, L. I. Sukhomlinova, and R. J. Twieg, Chem. Mater. **11**, 1784 (1999).
[34] M. Abkowitz, M. Stolka, and M. Morgan, J. Appl. Phys. **52**, 3453 (1981).
[35] M. Abkowitz, H. Bassler, and M. Stolka, Philos. Mag. B **63**, 201 (1991).
[36] R. Bube, *Photoconductivity of Solids* (Wiley, New York, 1960).
[37] *Photoconductivity in Polymers*, edited by A. Patsis and D. Seanor (Technomic Westport, CT, 1976).
[38] R. Blum, M. Sprave, J. Sablotny, and M. Eich, J. Opt. Soc. Am. B **15**, 318 (1998).
[39] P. Blom, M. de Jong, and M. van Munster, Phys. Rev. B **55**, R656 (1997).
[40] L. Bozano, S. Carter, J. Scott, G. Malliaras, and P. Brock, Appl. Phys. Lett. **74**, 1132 (1999).
[41] T. Daubler, D. Neher, H. Rost, and H. Horhold, Phys. Rev. B **59**, 1964 (1999).
[42] M. Pauley, H. Guan, and C. Wang, J. Chem. Phys. **104**, 6834 (1996).
[43] W. E. Moerner, S. M. Silence, F. Hache, and G. C. Bjorklund, J. Opt. Soc. Am. B **11**, 320 (1994).
[44] E. Hendrickx, B. Kippelen, S. Thayumanavan, S. Marder, A. Persoons, and N. Peyghambarian, J. Chem. Phys. **112**, 9557 (2000).
[45] P. Marcus and P. Siders, J. Phys. Chem. **86**, 622 (1982).
[46] R. Young, J. Chem. Phys. **103**, 6749 (1995).
[47] P. Borsenberger and D. Weiss, *Organic Photoreceptors for Imaging Systems* (Marcel Dekker, New York, 1993).
[48] W. E. Moerner, A. Grunnet-Jepsen, and C. Thompson, Annu. Rev. Mater. Sci. **27**, 585 (1997).
[49] A. Blythe, *Electrical Properties of Polymers* (Cambridge University, Cambridge, England, 1979).
[50] J. Slowik and I. Chen, J. Appl. Phys. **54**, 4467 (1983).